PARTICULATE FORMATION FROM PULVERIZED COAL UNDER OXY-FUEL COMBUSTION CONDITIONS

by

Yunlu Jia

A thesis submitted to the faculty of
The University of Utah
in partial fulfillment of the requirements for the degree of

Master of Science

Department of Chemical Engineering

The University of Utah

August 2015

The University of Utah Graduate School

STATEMENT OF THESIS APPROVAL

The thesis of **Yunlu Jia**

has been approved by the following supervisory committee members:

JoAnn S. Lighty	, Chair	**08/11/2011** Date Approved
Jost O.L. Wendt	, Member	**08/11/2011** Date Approved
Adel F. Sarofim	, Member	**08/11/2011** Date Approved

and by **JoAnn S. Lighty** , Chair of the Department of **Chemical Engineering**

and by David B. Kieda, Dean of The Graduate School.

ABSTRACT

Aerosol particulates are one of a variety of products generated by coal combustion. The objectives of this study were to elucidate ash particulate formation during oxy-fuel pulverized coal combustion compared to O_2/N_2 combustion. Oxy-fuel coal combustion conditions provide exhaust gas with a high concentration of CO_2 versus CO_2/N_2 due to the recycled flue gas. Understanding fine particle formation is important for predicting emissions and understanding potential deposition.

The hypothesis for CO_2 affect the particulate formation is that this high CO_2 concentration reduces the vaporization of refractory oxides from combustion according to the reaction: $MO_n(s) + CO(g) \longleftrightarrow CO_2(g) + MO_{n-1}(g)$. This research experimentally investigated particulate formation in a laboratory laminar flow drop tube furnace with well controlled combustion conditions under different flue gas scenarios. Ash particulate formation has been studied as a function of temperature, coal type, and gas phase conditions, namely, CO_2 versus N_2. Two bituminous coals, Utah Skyline and Illinois #6, and one sub-bituminous coal, Powder River Basin (PRB) black thunder were reported. During the experiments, the furnace temperature was set at 1373 K and 1500 K to study the effect of the combustion temperature on particle size distributions (PSDs).

A single particle model was developed for coal char to predict char particle temperatures and to illustrate the temperature differences between conditions. A Scanning Mobility Particle Sizer (SMPS) and an Aerodynamic Particle Sizer (APS) were utilized for ash PSDs in size ranges between 14.3 nm to 20 microns. In addition, particles were collected on an eleven-stage, Berner Low Pressure Impactor (BLPI) for elemental analysis using Scanning Electron Microscopy (SEM) and Energy Dispersive Spectroscopy (EDS).

It is found that temperature was the driving mechanism for increasing the amount of ultrafine formation. Increases in predicted particle temperature yielded

an increase in mass. As a second order effect, the combustion in an O_2/CO_2 environment yielded smaller masses of ultrafine particles than combustion in an O_2/N_2 environment. EDS results supported the SMPS/APS data as well and showed that, as expected, the coarse composition did not change significantly for the coals, but the ultrafine compositions were dependent upon the silicon, for Utah, and calcium, for PRB.

CONTENTS

LIST OF FIGURES

LIST OF TABLES

CHAPTER 1

INTRODUCTION

1.1 Motivation

1.1.1 Oxy-fuel Combustion

The world currently depends on fossil fuels for its energy supply, and this will continue for the foreseeable future. According to the reports from World Coal Institute (2006) and International Energy Agency (2007), 25% of global primary energy needs and 40% of the world's electricity generation are from coal combustion, which is more than twice the individual contributions from natural gas, nuclear, the hydroelectric sources and etc. Coal is the cheapest and largest readily accessible source of fossil energy for electricity generation. The USA consumes about 14% of the world's coal, using 90% of it for generation of electricity. In the worldwide, the United States is responsible for over 27% of the electric power generated by combustible fuel, with China having a 13% share, provided by Energy Information Administration (2005). However, CO_2 emissions from the combustion of fossil fuels are a dominant contributor to greenhouse gas emissions. Continued use of coal for electricity generation will require reduction of CO_2 emissions. Oxy-fuel coal combustion is a promising CO_2 capture technology for pulverized coal-fired power plants, reported by Buhre et al. [12], Nsakala et al. [36]. Oxygen mixed with recycled flue gas replaces air combustion resulting in a flue gas that consists primarily of CO_2, which is readily CO_2 captureable. The principle of oxy-fuel combustion of e.g., lignite in a pulverized fuel boiler is shown in Figure 1.1.

1.1.2 The Impact of Pulverized Coal Combustion to the Environment

Another important environmental issue from coal combustion is the emission of ash particulates. The research from Linak and Wendt [32] showed that the release of semivolatile trace metals generated from coal-fired power plants has

become a great challenge to the environment. Block et al. [11] reported that coal combustion is responsible for the large amount emission of particulates into the atmosphere; due to the ash content of coal are approximately two orders of magnitude higher than that of fuel oil. The fly ash produced by coal combustion contains high concentration of both the inorganic and organic components of the original coal. The concentrations of which are commonly enriched by about a factor of ten compared to the original coal. The ash particulates have a size range from several nanometers up to 100 microns. Particles in these size ranges are of the most concern, for they are not completely captured in pollution reduction equipment. The ash particles contain iron and other refractory metals, which have various harmful effects on human health, according to the studies from Bachmann et al. [3], Dockery et al. [15] and Lighty et al. [30]. Xie et al. [53] found that emissions of fine ash particles and some toxic elements from coal combustion are closely associated because the fine particles tend to be considerably enriched in trace elements. Particulates, when inhaled, can scratch and damage the respiratory system, causing acute and/or chronic respiratory illnesses. Depending on their chemical composition, they can contribute to other adverse health effects. Buhre et al. [12], [13] concluded that the need to control the emission of fine particulates with an aerodynamic diameter of less than 10 μm (PM_{10} emissions), together with their trace element content, is therefore a high priority in many countries.

Trace metals exist during the whole process of coal combustion. Trace metals can be distributed at different particle sizes and species depending on the combustion conditions. Trace metals contained in the fine particles are of the most concern due to the limited collection efficiency for fine particles for both electrostatic precipitator and filter bag control equipment. The fine particles have a about 100–1000 hours mean residence time, about 10 times that of supermicron particles, found by Esmen and Corn [17]. Therefore, the higher the emission of fine particles from pulverized coal combustion, the higher the risk of trace element for human respiratory systems. Many industrialized nations have passed regulations to limit particulate emissions. In the U.S., two sets of regulations govern air emissions of metal emissions from combustion systems, including hazardous waste and municipal waste incinerators.

One regulation is the Resource Conservation and Recovery Act (RCRA) [16], which regulates metal emissions based on risk assessments and limits the ground level concentrations inhaled by the most exposed individual. The other one is the Clean Air Act Amendments (CAAA) [1], which regulate the limitation on the emissions of 189 organic and metallic hazardous air pollutants, including air emissions from varieties of combustion sources. Understanding the mechanisms of Particulate Matter (PM) formation under oxy-fuel combustion conditions is important for its prediction and regulation.

1.2 Ash Formation Mechanism

The formation of fine ash particles in the coal combustion system affects the emissions of toxic metals and the formation of furnace deposits. The formation of micron size aerosols during coal combustion is caused by mineral vaporization under local combustion conditions and subsequent particle formation. Quann and Sarofim [38], Senior and Flagan [43] found that refractory metals vaporize during pulverized coal combustion, oxidize in the O_2/N_2 atmosphere and then diffuse away from the char particle. Diffused metallic oxide vapors encounter an O_2 rich environment and reoxidize to become saturated vapors. The saturation ratios could be so high that the amounts of ultrafine ash particles are formed by homogeneous nucleation. Then, these newly formed ultrafine particles grow in size by coagulation and heterogeneous condensation to become fine particles. The coarse size particles are mainly formed by char fragmentation and mineral coalescence. These large particles form directly from coal chars burnout. Padia et al. [41] found that the coalescence of molten minerals is considered as the primary formation mechanism of the coarse mode. Examinations of partially oxidized coal particles revealed that the condensation and abundance of molten minerals on the existing char or ash particle surfaces dominated the formation of the larger size particles, by Ramsden [40] and Kang et al. [27]. However, the mineral distribution inside char particles, strongly affected the coalescence process. At the experimental O_2 concentration conditions considered in this study, char particles are probably oxidized mainly on the external surface first, and then the particle is formed by

mineral condensation. A schematic presenting the current understanding of the ash particulate transformation is shown in Figure 1.2.

The important potential ash transformation mechanisms are summarized by Seames [42] as following:

1. Metal released from the solid matrix and subsequent vaporization;
2. Homogeneous nucleation occurred to form submicron particles;
3. Heterogeneous condensation/reaction of metal vapor occurred to form submicron particles;
4. Aerosol fume coagulated to form large particles;
5. Metal vapor condensed to be supermicron particles;
6. Metal vapor reacted with other chemical species on the surface of particle or in the pores of supermicron particles;
7. During these process, inclusion of ash particles formed during the process of combustion.

1.3 The CO_2 Effect in the Vaporization of Metal Element during Coal Combustion

Szekely et al. [50] suggested that chemical reduction should proceed through gaseous intermediates via the heterogeneous reactions:

$$MO_n(s) + CO(g) = CO_2(g) + MO_{n-1}(g) \tag{1.1}$$

$$MO(s) + CO(g) = CO_2(g) + M(g) \tag{1.2}$$

$$CO_2 + C = 2CO \tag{1.3}$$

Introducing CO_2 into the combustion environment and changing the combustion temperature would cause variations in vaporization, diffusion, oxidation, condensation, and nucleation, all of which affect ash formation. Based on the hypothesis that was originally developed by Quann [39], Haynes et al. [22], Neville et al. [35], and Kauppinen and Pakkanen [28]: vaporization of the refractory oxides

is governed by the following reaction: $MO_n(s) + CO(g) \longleftrightarrow CO_2(g) + MO_{n-1}(g)$. The vapor pressure of the vaporizing suboxides or metal (MO_{n-1}) is determined by the equilibrium of the reaction between the refractory metal oxides MO_n and CO inside the particle at high temperatures.

If the partial pressure of CO_2 in the bulk gas phase increases, the CO_2 will drive the reverse reaction. This means that vaporization rate of metal oxides will decrease. The equilibrium partial pressure of the metal or suboxide vapor, P^e_M, at the surface of char particle is determined from the equilibrium constant K_e from Equation 1.4:

$$K_e = \frac{P^e_M P_{CO_2}}{aMO_n P_{CO}}, \tag{1.4}$$

where *a* is the activity of metal oxide.

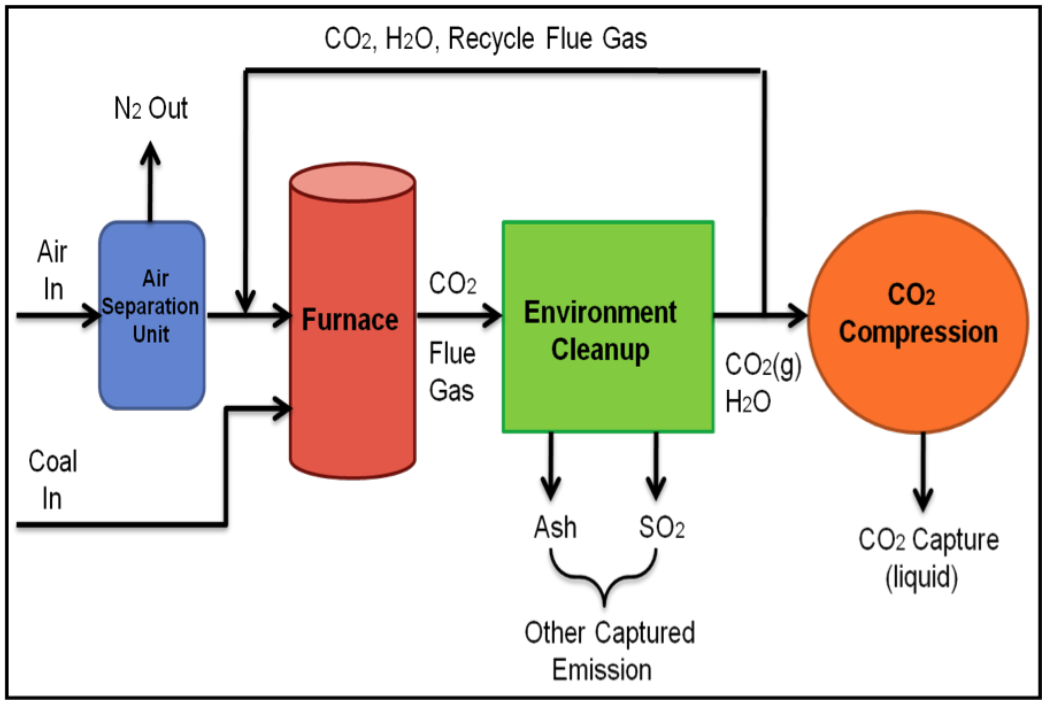

Figure 1.1: The principle of oxy-fuel combustion in a pulverized fuel boiler.

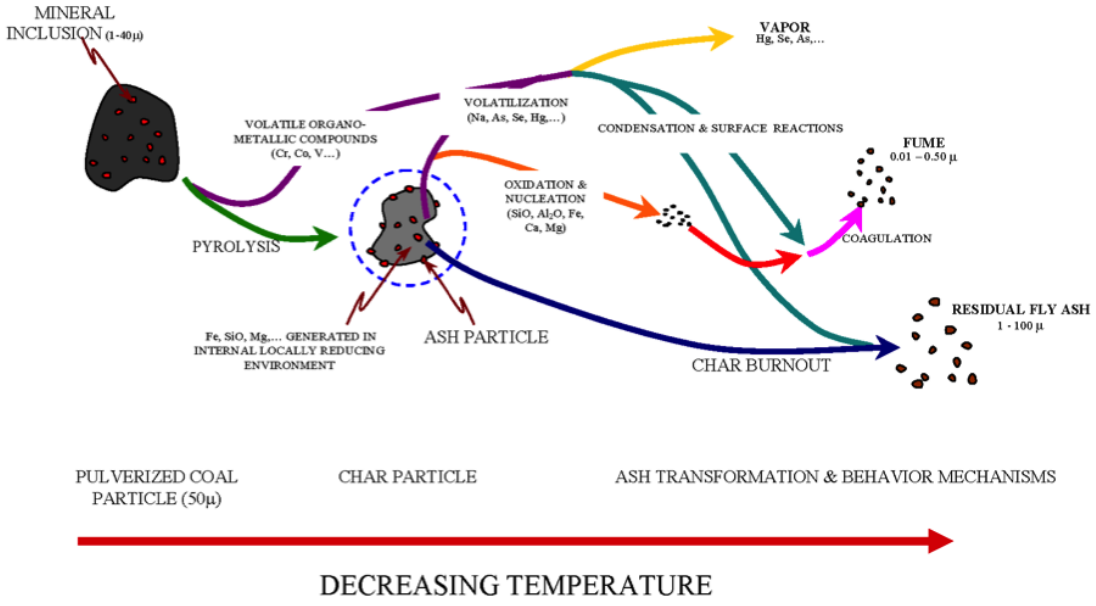

Figure 1.2: Transformation mechanisms in coal combustion.

CHAPTER 2

EXPERIMENTAL SETUP

2.1 Introduction

2.1.1 Drop Tube Furnace

The High Temperature Drop Tube (HTDT) furnace, built in 1974, was used for the ash formation studies. The furnace is capable of used for high-temperature, isothermal operation and well-controlled coal combustion and ash generation. It can operate at temperatures up to 1600 K, with an independently variable residence time, particle-feeding rate, and gas composition.

The heat was provided by an Astro model 1000A-3560 graphite element furnace. The heated section was 430 mm long. The first 170 mm served as a preheat section. An alumina honeycomb was set centrally at the last 50 mm of the preheat section to ensure laminar flow. The pulverized coal was fed into the furnace at an approximate rate of 1–2 g/hr. The furnace pressure was maintained at ambient pressure during all tests.

2.1.2 Feeding System

The coal particles were entrained by the N_2 carrier gas that flowed over the surface of an agitated coal bed and into a stationary test tube. A hypodermic steel tube with a 0.8 mm Internal Diameter (I.D.) was inserted over the bed. The end of the hypodermic was maintained closed to the surface of the coal bed to allow constant speed of coal feeding. The test tube was settled on a syringe pump that continuously pushed the test tube towards the hypodermic. The other end of the hypodermic was inserted into the water-cooled injection probe. A 5 cm distance of hypodermic tube above the end of the injection probe was maintained to prevent the hypodermic tube from heating up by radiation in the furnace. Coal particles would become softened and stick to the hypodermic walls, finally causing

unsteady coal feeding or coal particle plug. The particle feed rate was controlled by changing the speed of the syringe pump. 1–2 g/hr coal feeding rate was applied in experiments.

2.1.3 Furnace Modification

Some minor repairs were completed before experiments began, namely, collection probe remanufacturing, furnace modifications, and collection system alignment maintenance. The collection probe was more than 30 years old and had warped over the years. Its axis was no longer straight and did not align with the injection probe, making it unable to provide high collection efficiency. To obtain 85+% collection efficiency, a new collection probe was designed and built (Figure 2.1). As compared to the old collection probe, the diameter of the new probe was increased from 1.25" to 1.75", to increase the collecting area. As the products passed through the probe, they were quenched and diluted with N_2.

The top and bottom connecting flanges, which had recirculation water for cooling, were refabricated to meet the larger Outside Diameter (O.D.) alumina muffle tube, which was 3.25". The flanges were milled to have an I.D. of 3.27", allowing the outer alumina tube to move smoothly with the flanges. Unfortunately, the bottom flange had a water leak under high water pressure conditions after its four constructions. So, a new same flange was built to replace this broken one.

The old collection probe had just one supporting flange making the central line difficult to maintain. One stub flange was welded to the supporting flange and then connected to the other stub flange by O-ring and clamps. The new flange was constructed from aluminum and not water cooled to keep a low weight. A more precise positioning of the collection probe is well maintained by these two flanges. The final collection efficiency reached over 90% after HTDT modifications.

Finally, the cooling water circulation system had been running for years without a thorough cleanup. Crystallization of solid salts, oxides and hydroxides from the minerals in water, such as calcium and magnesium caused fouling. The fouling reduced the water flow and thermal conductivity efficiency, increased pressure drop and energy expenditure, and introduced additional heat to the system. Chemical and mechanical cleaning processes were performed to remove deposits

from the cooling water circulation system. In addition, the pipes and filters that had serious deposition were replaced. After the cleanup, the cooling water circulation system efficiency improved significantly. A high temperature test confirmed that the cooling water circulation system can protect HTDT running up to 1600 K. Figure 2.2 shows the overview of HTDT furnace with sampling system after modifications.

2.2 Sampling System

2.2.1 Scanning Mobility Particle Sizer (SMPS) and Aerodynamic Particle Sizer (APS) System

A TSI SMPS model 3080 and a TSI APS model 3321 were used for PSDs investigation. The SMPS has a theoretical measurement range of 14.3 to 673.2 nm. The APS was also applied to measure particle sizes ranging from 532 nm to 20 μm. Combining the SMPS and APS results yielded a measurement range of particles size from 14.3 nm to 20 μm. The measuring methods of these two instruments are different. For the SMPS, the sample passes through a charger that imparts a bipolar equilibrium charge to the particles. The charged aerosol enters the differential mobility analyzer where a fraction of the particles is selected according to its electrical mobility, which correlates with aerodynamic particle size. The selected fraction of the particles is counted in the condensation particle counter.

The APS counts particles by measuring the acceleration of aerosol particles in response to the accelerating flow field created by the inlet nozzle. The particle response to the accelerating flow field is dependent on its inertia and aerodynamic size. As the particle leaves the nozzle, its time-of-flight over a given distance depends on its aerodynamic size. The time-of-flight of the particle is found from the scattered light, which appears when the particle crosses the laser beams.

A quarter inch sampling probe was placed down to the collection probe outlet to obtain quenched sample. All samples drawn through the sampling probe were drawn and diluted with clean air in a dilution tunnel, in which the sample flow rate was held constant while the clean air flow rate varied, resulting in varied dilution ratios. In these experiments, two dilution ratios were tested, 1:17.8 and 1:22.2. The dilution tunnel contained sample ports for the particle sizing instruments (SMPS and APS).

2.2.2 The Berner Low Pressure Impactor System

Gravimetric measurements were collected to confirm the PSDs. Samples extracted by the collection probe from the furnace were routed through a Berner Low Pressure Impactor (BLPI) using a N_2 dilution gas and vacuum pump, more details were discussed by Hillamo and Kauppinen [24]. The BLPI was originally designed by Berner [8], [9] at the University of Vienna. The bottom stage of the BLPI worked as a sonic orifice to control the total flow rate flowing through the BLPI. During the experiments, the total gas flow rate for BLPI was maintained at a constant value of 25.4 slpm (standard liters per minute). The combustion gas was diluted at 1:12.7 in BLPI. The BLPI uses low pressure and high jet velocities for particles size segregation, which collects particles on 11 stages with particle sizes as follows (50% aerodynamic cutoff diameter–in microns): 15.7 (stage 11), 7.33, 3.77, 1.98, 0.973, 0.535, 0.337, 0.168, 0.0926, 0.0636 and 0.0324 (stage 1, bottom).

Particulate samples were collected on greased alumina foils in the BPLI for gravimetric measurements. To collect sufficient mass of ultrafine particles for measurements, the BLPI was operated in two steps. First, a cyclone was attached to the outlet of collection probe to remove particles larger than 1 μm, which were collected from stage 7 to stage 11. Operation with cyclone lasted about 180 min to ensure sufficient ultrafine particles were collected on the bottom stages, without overloading the larger particle stages. Then, the cyclone was removed to allow the BLPI collected larger particles on the upper stages. The whole PSD was obtained by combining results from both BLPI operating modes.

2.2.3 The Scanning Electron Microscopy (SEM) and Energy Dispersive Spectroscopy (EDS) System

Particulates were also collected on polycarbonate membranes in the BLPI for morphology and elemental analysis. The BLPI was applied for 15–20 min to allow a few particles to deposit on each impactor stage. Samples were examined by a FEI Nova Nano SEM and an Energy Dispersive X-ray detector (EDAX). The SEM ran at 0.3 torr water vapor low vacuum with Low vacuum high contrast detector (vCD) for morphology observation. The accelerating voltage used for morphology was 7 kV, the beam current was set to 22 pA, and the working distance was 6

mm. This small beam current and short working distance would improve imaging resolution at high magnifications. Low Vacuum Detector (LVD) was replaced by vCD detector for elemental analysis. The accelerating voltage increased to 15 kV for identification of high atomic number element, such as Fe. Seven main elemental oxides were analyzed for the eleven ash samples, including major elements, Na, Mg, Al, Si, S, Ca and Fe (reported as oxides). An elemental size distribution of PM generated by burning Utah Skyline, PRB and Illinois #6 coals at 1500 K in O_2/N_2 and O_2/CO_2 atmospheres were studied. Elemental distribution is presented as the weight percentage of the major elemental oxides as a function of particle size, and the mass distributions of particulates on stage 1 to 10 are also presented.

2.3 Coal Characteristics

Two bituminous coals and one sub-bituminous coal were studied: Utah Skyline, Illinois #6 and Powder River Basin (PRB), respectively. The coals were pulverized and sieved to 52–72 μm in the laboratory. The properties of all three coals were tested by Huffman Laboratories, Inc, are summarized in Table 2.1. The coals were dried at 105°C before testing to ensure continuous and stable feeding. Dried coal was introduced from the top of the furnace by a vibrating feeder at approximately 1–2 g/hr. Pulverized coals were burned in the HTDT furnace. The ash particulates generated from coal combustion were isokinetically collected and quenched by collection probe.

The incomplete combustion of Utah Skyline coal was observed in previous experiments, resulting in soot with ash product. The residence time was increased by decreasing the coal feed rate, gas flow rate (still keeping high excess O_2) and increasing the reaction zone (adjusting the position of the collection probe) to ensure that the coal combusted completely. Analysis with a photo-acoustic analyzer confirmed that there was no soot in the particulate collected in the long residence time experiments. The residence time was approximately 0.91 s to achieve complete combustion.

2.4 Experimental Conditions

An O_2/CO_2 mixture was used as the oxidant in the HTDT experiments to simulate O_2/recycled flue gas combustion, and these results were compared with the O2/N2 combustion conditions. During the experiments, the furnace temperature was set at 1373 K and 1500 K to study the effect of the combustion temperature on PSDs. Two O_2 concentrations, 21% and 31.5%, were used to investigate the gas composition effects. The experimental conditions are shown in Table 2.2.

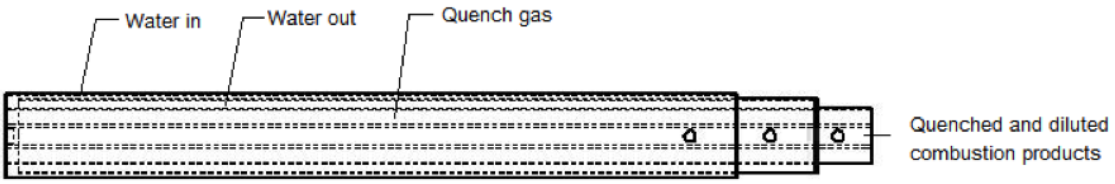

Figure 2.1: The side view of the collection probe.

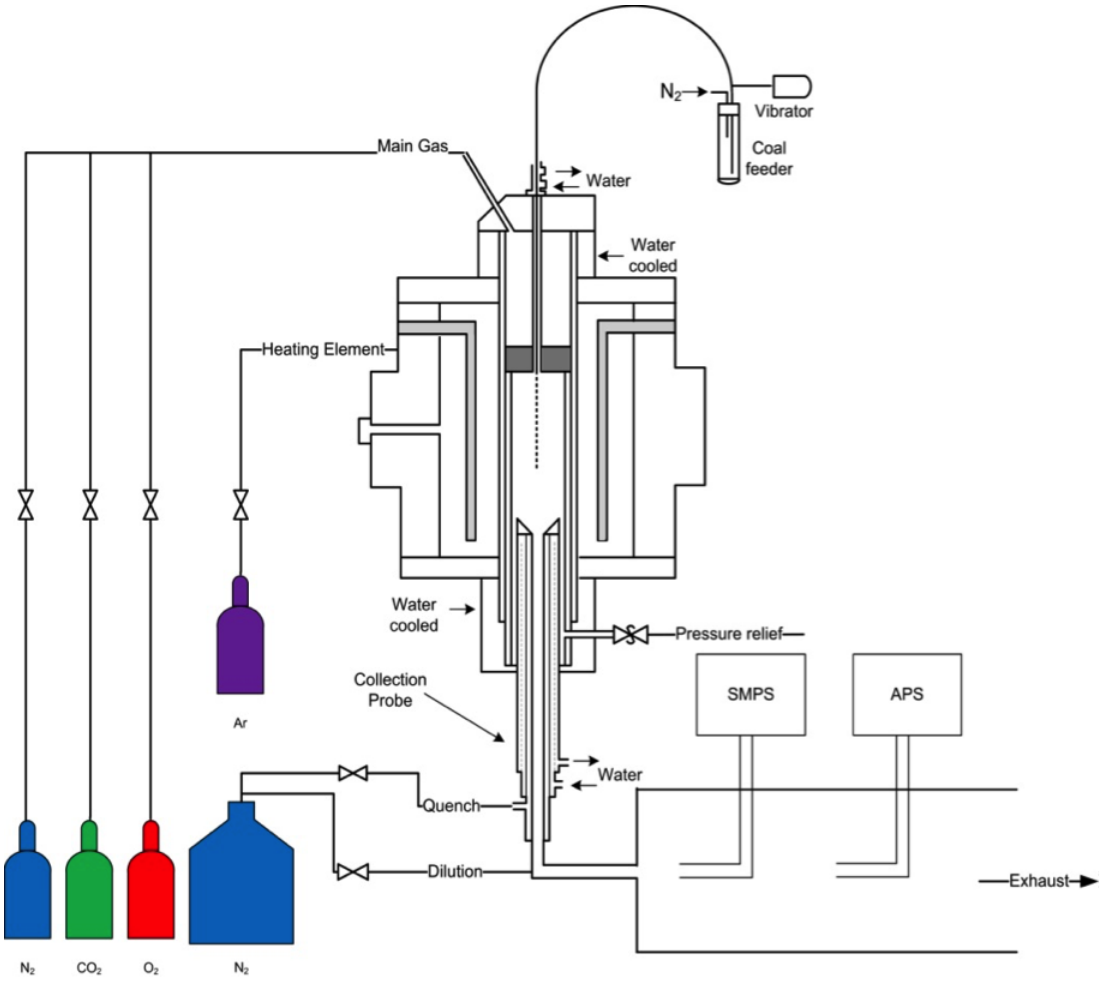

Figure 2.2: The overview of drop tube furnace.

Table 2.1: Coal analysis data for Utah Skyline, PRB and Illinois #6 coals.

	LOD[1] 105°C	Ash 750°C	C	H	N	S	O by diff.	Volatile Matter	Fixed Carbon	HHV[2]	
	%	%	%	%	%	%	%	%	%	BTU/lb	
Utah Skyline	3.18	8.83	70.6	5.41	1.42	0.53	13.21	38.6	49.39	12606	
PRB	23.69	4.94	53.72	6.22	0.78	0.23	34.11	33.36	38.01	9078	
Illinois #6	9.65	7.99	64.67	5.59	1.12	3.98	16.65	36.78	45.58	11598	
Ash Analysis[3]											
	Al	Ca	Fe	Mg	Mn	P	K	Si	Na	S	Ti
	as Al_2O_3	as CaO	as Fe_2O_3	as MgO	as MnO	as P_2O_5	as K_2O	as SiO_2	as Na_2O	as SO_3	as TiO_2
Utah Skyline	14.52	6.11	5.09	1.39	0.02	0.59	0.57	60.89	1.41	2.33	0.88
PRB	14.78	22.19	5.2	5.17	0.01	1.07	0.35	30.46	1.94	8.83	1.3
Illinois #6	17.66	1.87	14.57	0.98	0.02	0.11	2.26	49.28	1.51	2.22	0.85

[1] LOD: Loss on drying determined in air at 105°C for 1 hour and is reported on an as received sample weight basis.
[2] HHV: higher heating value.
[3] Ash analysis results are reported on an ashed sample weight basis after stage ashing in air overnight at 750°C.

Table 2.2: Combustion conditions.

Furnace Temperature	Gas Composition	Oxygen Ratio
1373 K	O_2/N_2	21%
		31.5%
	O_2/CO_2	21%
		31.5%
1500 K	O_2/N_2	21%
		31.5%
	O_2/CO_2	21%
		31.5%

CHAPTER 3

SIMULATION

3.1 Single Coal Char Particle Temperature Simulation Model

Previous experimental results suggest that coal combustion temperature would be a major potential reason to explain how ash forms during the combustion process. The ash vaporization rate also correlates to particle burning rate, which is affected by initial size of the coal.

The overall vaporization inside of the porous char is considered as a combination of all mineral volatilization after the coal ignites and with the temperature rise. The single mineral vaporization was shown in Figure 3.1.

The objective of the simulation is to elucidate all factors that affect the coal combustion temperature; the intent of the model was not to fully describe the conditions but show differences between conditions. Understanding the temperature of coal particle combustion for a certain set of furnace conditions is important to understand the kinetics of ash vaporization process. The combustion of pulverized coal particle has been studied both on the theoretical and experimental fields, such as Smith [46], Mulcahy and Smith [34], and Simons [45]. According to the investigations of Howard and Essenhigh [25], and Altricher [2], the occurrence of vaporization, combustion, nucleation and condensation of the volatile mineral is simultaneous with the heterogeneous combustion of the char particle. This process depends on temperature, heating rates, particle size and other possible factors.

The combustion temperature and burnout rate of an individual coal char particle are determined by furnace temperature, bulk gas composition, coal type and char particle size using detailed mass transfer, thermodynamics, reaction kinetics and heat transfer calculations. The model presented below assumes the following: spherical, homogeneous particle, reactions in the boundary layer are negligible, and

there is no temperature gradient within the particle. More details were discussed by Badzioch [4] and Carslaw [14]. For the predicted combustion temperatures and burnout times, gas diffusivities and thermal conductivities were estimated using the Chapman-Enskog kinetic theory of gases by Bird, Stewart and Lightfoot [10]. Smiths' [47] intrinsic kinetics was used assuming a first order reaction rate with respect to oxygen concentration.

The reaction considered in the simulation is: $2\,C(s) + O_2(g) \longrightarrow 2\,CO(g)$.

In this calculation the only reaction considered at the char particle surface was the direct oxidation of carbon to form carbon monoxide, $2\,C + O_2 \longrightarrow 2\,CO$, following the approach of Field [18], Gavalas [19], and supported by the findings of Tognotti et al. [51]. Gas-phase oxidation of CO to CO_2 was assumed to occur in the free stream and therefore did not enter into the energy and material balance equations.

Both the diffusional coefficient and reaction coefficient were considered for the burning rate computation. The thermodynamic properties of char particle and bulk gas mixture were calculated at each change in temperature. All three coals, Utah Skyline, PRB and Illinois #6 were used for the simulation. The reaction rates of these three coals were assumed to be the same; the differences among these three coals were mainly their physical properties and heating values. The simulation conditions used in the study are the same to the experimental studies. A size of 65 μm char particle was applied for the simulation.

A schematic of the heat balance on the surface of the coal char particle is shown in Figure 3.2.

The following heat balance expression can be used and it gives the rate of change of particle temperature with time:

$$\underbrace{m_p C_p \frac{dT_p}{dt}}_{①} = \underbrace{-\epsilon\sigma A_p \left(T_p^4 - T_w^4\right)}_{②} \underbrace{- hA_p \left(T_p - T_g\right)}_{③} + \underbrace{\Delta H_\gamma}_{④} \tag{3.1}$$

The term represents the change of particle temperature with time:

$$m_p = \rho \frac{4}{3} \pi d_p^3, \tag{3.2}$$

where m_p: particle mass (kg),
d_p: particle diameter (m),
ρ: particle density (kg/m^3),
C_p: specific heat of the particle (J/(kg·K)),
T_p: particle surface temperature (K),
t: time (s).

Baughman [5] mentioned that the coal density is variable and dependent on the coal type. The true density can be determined by the elemental composition of coal. Speight [49] described this expression to calculate the density of coal

$$\rho = 1.534 - 0.05196H + 0.007375O - 0.02472N + 0.003853S. \tag{3.3}$$

The calculated densities of Utah Skyline, PRB and Illinois #6 coal are 1531.8, 1553.1, and 1532 kg/m^3, respectively. The estimation of the specific heat of coal is based on Kopp's law. Incropera [26] used this expression for computing specific heating that applies according to elemental analysis of coal

$$C_p = 0.189C + 0.874H + 0.360O + 0.491N + 0.215S \quad \text{Btu/(lb} \cdot {}^\circ\text{C)}, \tag{3.4}$$

where C, H, N, O, and S are the respective weights (% w/w) of the elements in the coal. The calculated specific heat of Utah Skyline, PRB and Illinois #6 coals are 992.9, 1188.6 and 1042.4 J/(kg·K), respectively.

The term gives heat loss by radiation, where
ϵ: particle emissivity, usually uses 0.8 for coal particle,
σ: the Stefan-Boltzmann constant; its value is 5.67051×10^{-8} W/m^2·K^4,
A_p: the surface area of the particle (m^2), $A_p = 4\pi d_p^2$,
T_w: wall temperature (K).

The term is convective heat loss of the particle, where h is the convective heat transfer coefficient of the process, (W/m^2·K). The heat transfer coefficient, in the heat transfer equation is computed from $h = \frac{k_f \cdot Nu}{D_p}$; 2 is chosen for the Nusselt number. The thermal conductivity of the gas k_f increases with temperature increases, and it is assumed that the thermal conductivity is proportional to the absolute temperature to the power of 0.75. Thermal conductivity of O_2, CO_2 and

N_2 are different. The value of thermal conductivity is calculated for gas mixture based on their concentration. Field et al. [18] gave this expression for thermal conductivity calculation

$$k_f = k_{f0} \cdot \left[\frac{T_g + T_p}{2T_0} \right]^{0.75}, \tag{3.5}$$

where k_{f0}: the reference mean thermal conductivity of gas around the particle.
T_0 is the reference temperature, assumed as 900 K in the calculation.

The value of thermal conductivity of each gas species is from the National Institute of Standards and Technology (NIST) database [29].

The term is heat generated from chemical reaction, where
ΔH: heat release at particle surface per unit mass of char combustion $2\,\mathrm{C(s)} + \mathrm{O_2(g)} \longrightarrow 2\,\mathrm{CO(g)}$, kJ/kg. Assuming only CO is generated in the combustion process, 111kJ/mol-C, which is 9.25 MJ/kg-C, from Mcbride and Gordan [21] and Weast [52], is used for value of reaction heat releasing.
γ is the overall reaction rate, kg/s. There are two models used to estimate reaction rate on particle surface reaction.

The Baum and Street [6] developed a kinetic/diffusion surface reaction rate model, based on apparent activation energy; while Smith et al. [48] and Field et al. [18] derived a more fundamental intrinsic reactivity model.

In this simulation, both oxygen diffusional reaction rate from bulk gas to particle surface and particle surface reaction rate are considered for overall reaction rate determination. The oxygen diffusion rate coefficient is calculated by $k_d = \frac{24\varphi D_{O_2}}{2D_p R' T_m}$, kg/(m$^2 \cdot s \cdot$atm$O_2$), where
T_m: mean temperature between particle surface and gases, $T_m = \frac{T_p + T_g}{2}$,
φ: a mechanism factor, 2 for CO is transported away from particle surface, and 1 for CO_2 is transported,
R': gas constant, 82.06 atm·cm^3)/(g-mol·K),
D_{O_2}: oxygen diffusion coefficient in binary gas mixtures, cm^2/s, using the Chapman-Enskog theory to estimate the diffusivity of the O_2/N_2 or O_2/CO_2 system at combustion temperature and pressure condition.

The Chapman-Enskog theory predicts the diffusion coefficient of a gas pair in cm^2/s according to the formula, $D_{O_2} = \frac{0.00266 T_m^{3/2}}{P M_{bi}^{1/2} \sigma_{bi}^2 \Omega_D}$, by Marrero and Masion [33],

where P: gas pressure, bar. 1 atm = 1.01325 bar,

M_{bi}: molecular weights of binary gas mixtures, $M_{bi} = 2\left[\frac{1}{M_1} + \frac{1}{M_2}\right]^{-1}$, kg/mol,

σ_{bi}: Characteristic length, Å,

Ω_D: Diffusion collision integral, dimensionless.

More details are discussed in Poling's book [37].

The particle surface chemical reaction rate coefficient is calculated based on Arrhenius equation,

$$k_p = Ae^{-\frac{E_A}{RT_p}}. \tag{3.6}$$

where A: frequency factor, kg/m^2·s·atmO_2,

E_A: activation energy, J/mol,

R: 8.3144 J/(mol·K), the universal gas constant.

The value of A and E_A are used from the experimental data by Geotz et al. studies [20].

The overall reaction rate coefficient per unit particle surface area at certain oxygen pressure is obtained by $k_o = \left[\frac{1}{k_d} + \frac{1}{k_p}\right]^{-1}$.The overall reaction rate depends on both k_d and k_p but tends to be dominated by the smaller one. Therefore, the diffusional term would dominate for large particles and at higher temperature, and the chemical reaction term would dominate for small particles and at lower temperature cases or hardly reactive fuels.

Assuming a heterogeneous surface reaction, the overall reaction rate at the particle surface is

$$\gamma = k_o \cdot P_{O_2} \cdot A_p, \quad \text{kg/s} \tag{3.7}$$

where P_{O_2} is the O_2 partial pressure around the char particle.

The rate of char mass loss by combustion, $\frac{dm}{dt}$, depends on particle density, diameter, and the particle surface overall reacting rate.

The description of coal consumption is calculated by

$$\frac{dm}{dt} = -\gamma. \tag{3.8}$$

The calculations of reaction rate γ were obtained from previous calculation.

All the parameters that are used in the simulation are listed in Table 3.1.

3.2 Simulation Results

The simulated temperature profiles of Utah Skyline combusted at 1373 K and 1500 K for both O_2/N_2 and O_2/CO_2 conditions are shown in Figure 3.3. The burnout time results of Utah Skyline are shown in Figure 3.4.

PRB and Illinois #6 have similar temperature and burn out time profiles as Utah Skyline simulation. The simulation results of all three coals were summarized in Tables 3.2 and 3.3.

Utah Skyline coal had the highest heating value, followed by Illinois #6 and PRB. The simulation results showed that the particle temperature of Utah Skyline was the highest and the burnout time was the shortest among these three coals at the same combustion conditions. Both increasing the furnace wall temperature and increasing oxygen concentration in the combustion gas increased coal char particle combustion temperature and lowered the burnout time.

Compared with O_2/N_2 and O_2/CO_2 combustion conditions, the char particle combustion temperature in O_2/N_2 is higher than that in O_2/CO_2, and particle burnout time in O_2/N_2 is shorter than that in O_2/CO_2 combustion at the same furnace temperature and oxygen concentration conditions. The most likely reasons are the heat transfer coefficient of N_2 is higher than that of CO_2, and the mass diffusivity of O_2 in CO_2 is lower than that of O_2 in N_2. Both reasons lead to a lower particle burning temperature and an increase in the burn out time of O_2/CO_2 combustion compared to O_2/N_2 conditions.

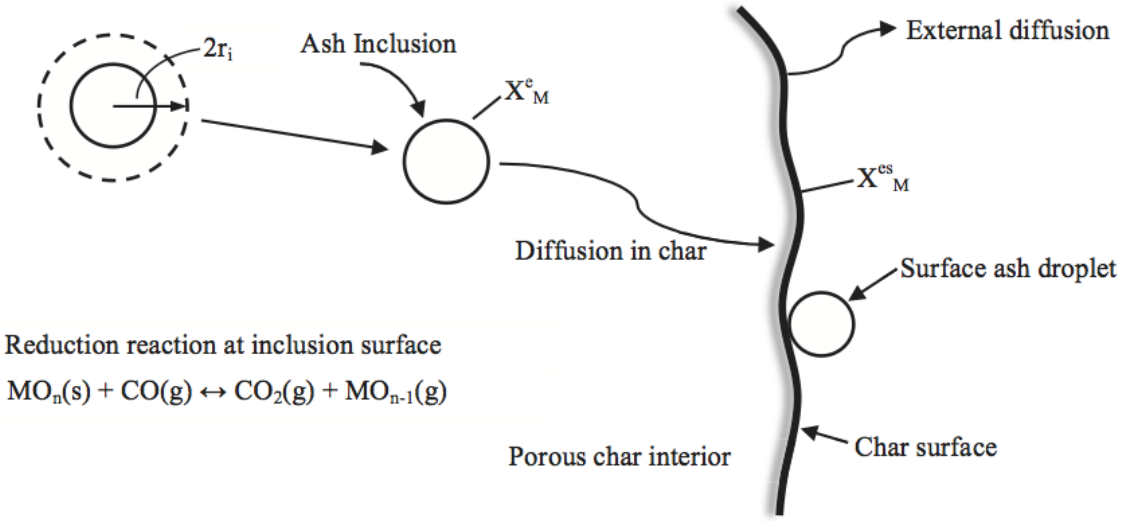

Figure 3.1: The mineral vaporization during coal combustion.

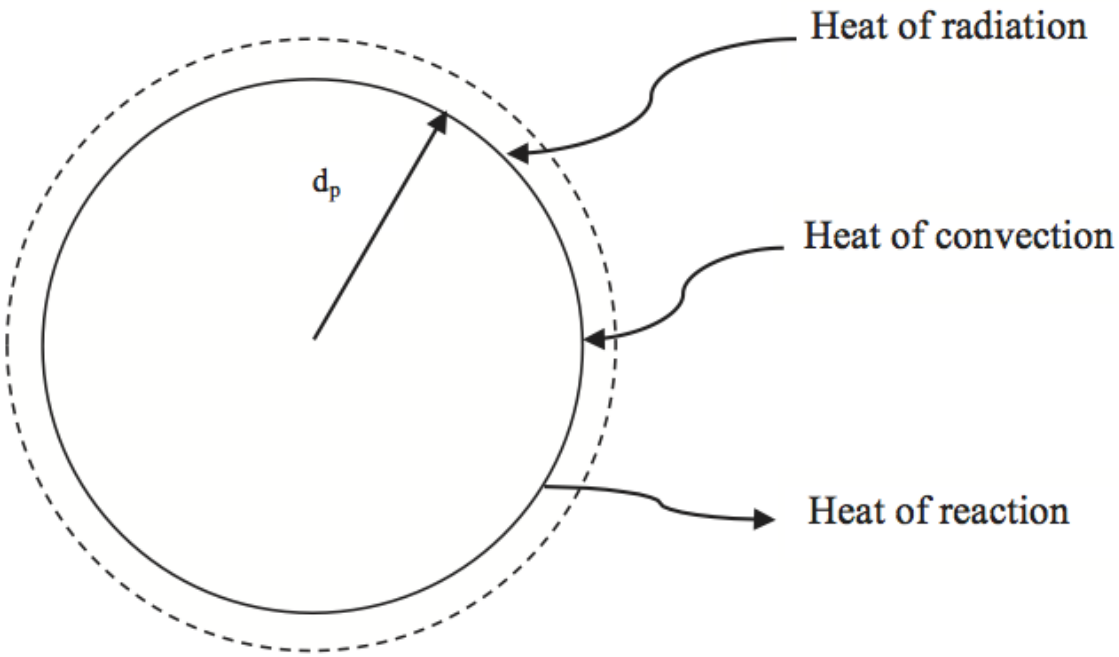

Figure 3.2: The heat balance on the surface of the coal char particle.

Table 3.1: Properties used in the simulation.

	Utah Skyline	PRB	Illinois #6
Coal Density *rho* (kg/m^3)	1531.8	1553.1	1532
Coal Specific heat C_p (J/kg·K)	992.9	1188.6	1042.4
Coal Emissivity ϵ	0.8		
Stefan-Boltzmann constant σ (W/m^2·K^4)	5.67E-08		
Ambient pressure P (atm)	1		
Molecular weight of C M_C (kg/mol)	0.012		
	O_2	N_2	CO_2
Thermal conductivity of gases k_f (W/m·K)	0.073	0.0607	0.0581
Molecular weight (kg/mol)	0.032	0.028	0.044
	O_2/N_2	O_2/CO_2	
Heat transfer coefficient h (W/m^2·K)	1500 ~ 4553	1460 ~ 4320	
O_2 diffusion coefficient (cm^2/s)	1.963 ~ 4.400	1.558 ~ 3.511	
Frequency Factor A (kg/m^2·s·atm O_2)	600		
Activation energy E (cal/mol)	15700		
Universal gas constant R (cal/mol·K)	1.986, 82.06 (atm·cm^3/g-mol·K)		
Coal particle diameter (μm)	50, 100		
O_2 volume percentage x_{O_2}	21%, 31.5%		
Initial temperature T_0 (K)	900		
Wall Temperature T_w (K) ($T_w = T_g$)	1373, 1500		
Heating release value (MJ/kg-C)	9.25		

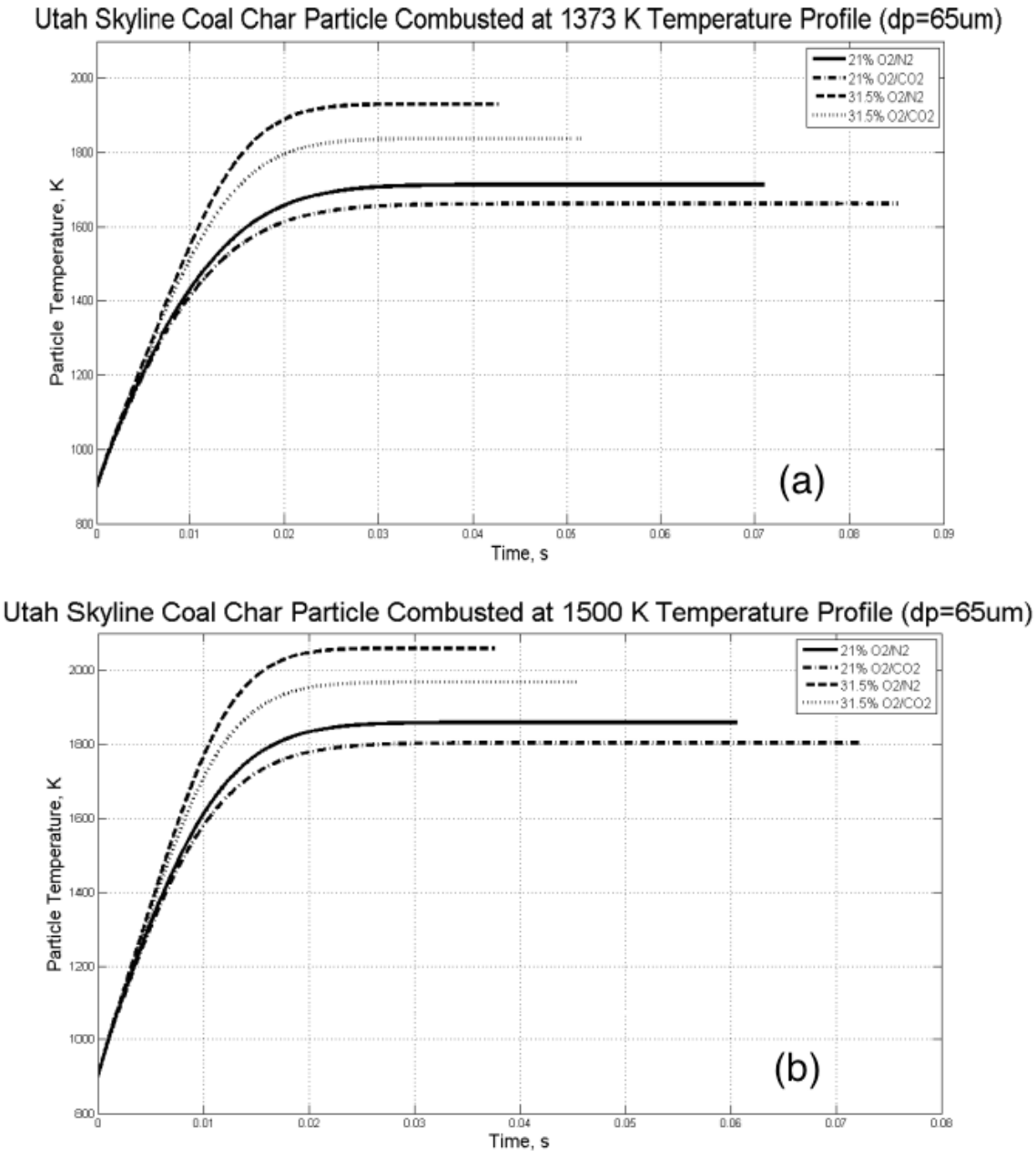

Figure 3.3: Utah Skyline coal char combustion temperature profiles at 1373 K (a) and 1500 K (b).

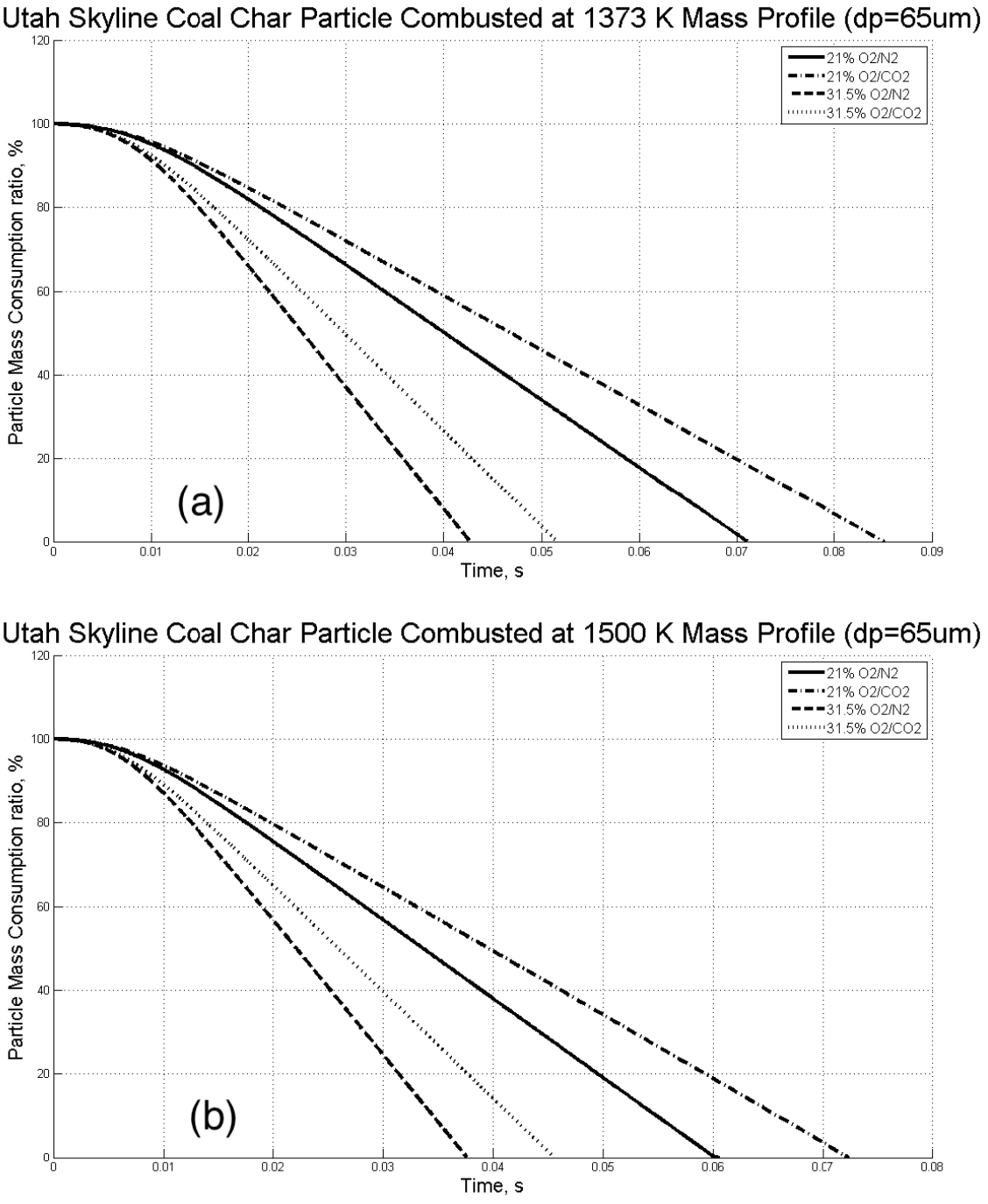

Figure 3.4: Utah Skyline coal char combustion burnout time profiles at 1373 K (a) and 1500 K (b).

Table 3.2: Coal char burnout time at the initial stage for particle diameter of 65 μm (s).

	Utah Skyline				PRB				Illinois #6			
	1373 K		1500 K		1373 K		1500 K		1373 K		1500 K	
O_2 volume (%)	21	31.5	21	31.5	21	31.5	21	31.5	21	31.5	21	31.5
O_2/N_2	71	42.7	60.6	37.7	81	49.2	66.2	42	73.9	44.5	63.6	38.9
O_2/CO_2	85.1	51.6	72.4	45.6	94.9	58.3	78.7	50	88	53.5	74.3	46.9

Table 3.3: Coal char combustion peak temperature at the initial stage for particle diameter of 65 μm (K).

	Utah Skyline				PRB				Illinois #6			
	1373 K		1500 K		1373 K		1500 K		1373 K		1500 K	
O_2 volume (%)	21	31.5	21	31.5	21	31.5	21	31	21	31.5	21	31.5
O_2/N_2	1714	1931	1859	2060	1613	1776	1764	1917	1679	1879	1827	2012
O_2/CO_2	1662	1838	1804	1968	1580	1711	1725	1850	1634	1795	1778	1929

CHAPTER 4

EXPERIMENTAL RESULTS

4.1 Measurements of PSDs with the SMPS/APS and BLPI

Figure 4.1 illustrates the PSD results of Utah Skyline combusted under 21% O_2 combined with CO_2 at a furnace temperature of 1500 K. The PSDs obtained from SMPS and APS instruments are compared to gravimetric determination of fly ash samples segregated and collected using a BLPI. Valid scans were used for SMPS/APS PSDs 15 times, and about 5 times running in BLPI. Both SMPS/APS and BLPI data were within one standard deviation analysis. The standard deviation implies the diversity of PSDs at each particle size. The PSDs agreed well in the region where SMPS and APS overlap. The combined PSDs covered the ultrafine mode, fine mode and coarse modes, from 14.3 nm up to 20 μm, more discussions in papers of Baxter [7], Helble and Sarofim [23], Smith et al. [48], and Linak et al. [31], [32]. The ultrafine mode is defined from 14.1 nm to the first lowest mass concentration value of PSD; the fine mode started from this point to next lowest mass concentration value of PSD; and the last part is the coarse mode. The BLPI data showed the same trend as the SMPS/APS data, with some scatter at the smaller particle sizes. This is likely due to the limited sample size for these smaller particles. The graph presents that the PSDs can be obtained from two independent measurements.

4.2 Ash Particle Size Distribution

All PSD data for Utah Skyline, PRB and Illinois #6 were derived from SMPS and APS measurements. The total mass was obtained by integrated the PSDs. Mean sizes—particle diameter:D_p and mass distributions of ultrafine, fine and coarse modes are shown in Table 4.1. Note that total mass of each sample =

ultrafine mass + fine mass + coarse mass = 1000 mg/g_ash. The mean particle size under O_2/CO_2 combustion conditions was smaller in the ultrafine and fine particle modes as compared with O_2/N_2 combustion conditions, except Illinois #6. The most remarkable differences in mass distribution were in the ultrafine mode and fine modes over different conditions; coarse modes were not affected by different combustion conditions. Similar results were found in Sheng et al. [44].

The mean sizes of ultrafine particles for all three coals are shown in Figure 4.2. The total masses of ultrafine particles for all three coals are shown in Figure 4.3.

The mean sizes of fine particles for all three coals are shown in Figure 4.4. The total masses of fine particles for all three coals are shown in Figure 4.5.

4.2.1 Utah Skyline Results

The PSDs of Utah Skyline from SMPS and APS measurements are shown in Figure 4.6. The simulation results showed that increasing the O_2 concentration increased the particle combustion temperature by about 200 K in an O_2/N_2 combustion environment and by 150 K for an O_2/CO_2 combustion environment at a furnace temperature of 1500 K. The temperature increase due to O_2 was more pronounced at the lower furnace temperature, approximately 200 K. The PSD for a 31.5% O_2/N_2 environment always had the highest ultrafine particle yield. Small effect from furnace temperature was observed except at the lowest particle temperature. The change in the O_2 concentration significantly changed the ultrafine and fine PSDs. The yields of ultrafine and fine particles increased with increasing O_2 concentrations in both O_2/N_2 and O_2/CO_2 environments. The mean particle size in the ultrafine particle under O_2/N_2 combustion conditions had a mean size of 0.045 μm for a 31.5% O_2 concentration and 0.25 μm for a 21% O_2 concentration (Table 4.1, Figure 4.2). A shift to smaller size on ultrafine and fine particle mean size for O_2/CO_2 was observed for both O_2 concentrations.

Under the conditions studied, CO_2 always reduced vaporization for Utah Skyline coal. At the same O_2 concentration, combustion in a CO_2 environment produced fewer ultrafine particles than in an O_2/N_2 environment. The simulated particle temperature of 31.5% O_2/N_2 at 1373 K was similar to that of 31.5% O_2/CO_2 at 1500 K. Their mean particle sizes in the ultrafine mode were similar. The yield

of ultrafine particles in O_2/N_2 was 9.18 mg/g_ash, while that of O_2/CO_2 was 7.63 mg/g_ash (Table 4.1, Figure 4.3). This result supports the CO_2 effect hypothesis very well. The CO_2 effect was expected in Utah Skyline combustion because Utah Skyline has high content of silicon and aluminum, which are classified as refractory metallic elements. Simulated particle temperatures at 31.5% O_2/CO_2 and 1373 K and 21% O_2/N_2 at 1500 K were similar. However, experimental results showed that higher O_2 concentrations yielded larger quantities of ultrafine particles, which reflects higher vaporization rates even though CO_2 was present. Therefore, the ultrafine yield was highest for a N_2 environment and the higher O_2 concentration. Decreased content of ultrafine yield was always shown in CO_2 environment. The shape of the coarse particle PSD was almost identical for all combustion conditions at the same furnace temperature. For the fine particles, the highest number was also for N_2 conditions. To have a better understanding of the differences among different combustion conditions on ultrafine and fine particle modes, PSDs were plotted based on the method originally developed by Markowski and Ensor (1977) for reporting impactor results, shown in Figure 4.7. The concentration of ultrafine particles from 21% O_2/N_2 and 21% O_2/CO_2 were under 0.1 (mg_ash/g_ash), while that of 31.5% O_2/CO_2 was about 0.1 (mg_ash/g_ash), which is about 20% of the concentration of 31.5% O_2/N_2 combustion.

Figure 4.8 shows the results from the BLPI and EDS analysis. The PSD shapes are the same as SMPS/APS data. The mass distributions of larger particles were in similar positions for all combustion conditions. As previously discussed, Utah Skyline contains a high silicon content. The mass fraction of Si was highest in the coarse mode (from 1.98 to 7.33 μm). The yields of Si were highest under the 31.5% O_2/N_2 condition, followed by 31.5% O_2/CO_2, 21% O_2/N_2, and 21% O_2/CO_2. This is the same order as the predicted particle temperatures from the simulation (order is high to low). Both the O_2 concentration and combustion environment (CO_2 versus N_2) had significant effects on Utah Skyline coal ash formation, as reflected in the detailed elemental distribution.

4.2.2 PRB Results

The PSDs of PRB are shown in Figure 4.9. Similar observations were shown in the PRB results: there were significant differences in ultrafine and fine mode versus coarse mode. The simulated particle combustion temperatures for PRB coal were lower to those of Utah Skyline coal. The mean size of the ultrafine particle mode under O_2/N_2 combustion conditions was 0.07 μm for 31.5% O_2 and 0.05 μm for 21% O_2 conditions (Table 4.1, Figure 4.2). The O_2/CO_2 environment resulted in ultrafine particles with a smaller mean particle size, although their mean sizes were higher than Utah Skyline coal. The 31.5% O_2/N_2 condition always had the highest mass concentration of ultrafine and fine particles. Increasing the oxygen concentration from 21% to 31.5% increased the predicted particle combustion temperature by about 150 K in the O_2/N_2 environment and by 130 K in the O_2/CO_2 environment. The change in the O_2 concentration significantly changed the PSDs. The yields of ultrafine and fine particles increased with the increasing of O_2 concentration for both O_2/N_2 and O_2/CO_2 combustion environments. The simulated temperature of 21% O_2/N_2 at 1500 K had a similar result to that of 31.5% O_2/N_2 at 1373 K. A higher yield of ultrafine particles was found for the higher O_2 concentration condition.

The simulated particle combustion temperature for 31.5% O_2/CO_2 was 1850 K as compared to 1775 K for 31.5% O_2/N_2. The yield of ultrafine PM in the CO_2 environment was less than that in the N_2environment (Table 4.1, Figure 4.3). This result suggested that CO_2 effect hypothesis was well supported. The lower yield of ultrafine PM in the CO_2 environment was also found at lower temperature. However, the CO_2 effect was less pronounced at low temperature.

The shapes of the coarse particle curves were similar for all combustion conditions at the same furnace temperatures. Some differences associated with temperature were evident in this mode. Similar ultrafine and fine particle plots were used for PRB coals in Figure 4.10. The mass concentration of ultrafine particle of 31.5% O_2/N_2 was about three times higher than that of 21% O_2/N_2 and 21% O_2/CO_2 combustion conditions.

The size-segregated elemental composition from PRB combustion is shown in Figure 4.11. PRB coal has a high content of Ca and Si, and Ca is the predominant

ash compound. Ca is more easily vaporized than Si, and PSDs changes are probably a result of temperature changes. The yield of calcium oxide showed the same trend as the predicted particle combustion temperatures and ash total mass concentrations. Therefore, the elemental analysis of PRB ash also supports the effect of O_2 concentration and effect of CO_2 in ash formation during coal combustion.

4.2.3 Illinois #6 Results

The PSDs of Illinois #6 are shown in Figure 4.12. All of the Illinois #6 PSDs showed the three modes most clearly among the three coals. Ash from Illinois #6 also showed the greatest fraction of ultrafine and fine particles compared to the other two coals. Significant differences of mass concentration in ash formation behavior were observed in ultrafine and fine mode. The mean size of the ultrafine particles showed the particle temperature effect more clearly at 1373 K than at 1500 K. The mean particle diameter of the ultrafine mode for O_2/N_2 combustion was 0.04 μm for 31.5% O2 and 0.028 μm for 21% O_2 (Table 4.1, Figure 4.2). The mean sizes of ultrafine particles from O_2/CO_2 combustion were about the same as O_2/N_2 conditions. The coarse mode PSDs were similar at the same furnace temperature. The ultrafine, fine and coarse particles at the same O_2 concentration conditions had similar yields in both N_2 and CO_2 environments, except for the ultrafine mode at a furnace temperature 1373 K.

The simulated particle combustion temperatures were similar to Utah Skyline coal. Increasing the O_2 concentration from 21% to 31.5% increased the predicted particle combustion temperature by about 200 K under O_2/N_2 combustion conditions and 150 K in O_2/CO_2 combustion conditions. The change in the O_2 concentration significantly changed the PSD, in particular the yield of ultrafine particulate at higher O_2 concentrations has higher value even with CO_2 present. The simulated particle combustion temperature for 21% O_2/N_2 at 1500 K was similar to that of 31.5% O_2/CO_2 at 1373 K. However, the ultrafine particle concentration of 31.5% O_2/CO_2 at 1500 K is yielded 17.03 mg/g_ash, much higher than that of 21% O_2/N_2 at 1500 K with a yield of 6.72 mg/g_ash (Table 4.1, Figure 4.4).

The CO_2 effect was observed at lower temperatures. Predicted particle combustion temperature at 21% O_2/N_2 and 21% O_2/CO_2 at 1373 K were similar. An

environment of O_2/N_2 yielded 16.437 mg/g_ash, compared to 8.824 mg/g_ash for an O_2/CO_2 environment (Table 4.1, Figure 4.4). For the higher furnace temperature, corresponding to higher particle temperature, the effect of CO_2 was not significant. Figure 4.13 showed the ultrafine and fine particle plots for Illinois #6. Significant mass concentration differences were shown in low furnace temperature conditions, as Utah Skyline and PRB coal. Not much concentration differences were found in normal plots of ultrafine particles for same O_2 concentration combustion at N_2 and CO_2 environments.

The size-segregated elemental composition of Illinois #6 ash is shown in Figure 4.14. Illinois #6 has a high content of sulfur silicon and iron. The ultrafine and fine particle modes had large concentrations of sulfur, with almost no sulfur in the coarse mode. This implied the formation of sulfates during the coal combustion. More sulfur was found at lower O_2 conditions, both in N_2/CO_2 environments. Si and Fe in mass distributions showed more dependence on O_2 concentration versus the combustion environment (N_2/CO_2) for all stage samples, which was consistent with the PSDs.

4.3 Morphology of Ash Particulates

Ash particulate samples collected from the BLPI system were used to determine morphology by an FEI NovaNano SEM with vCD low vacuum detector. Utah Skyline, PRB and Illinois #6 coals combusted under 31.5% O_2; CO_2 and N_2 atmosphere at 1500 K were studied. Figures 4.15, 4.16, and 4.17 show SEM images of ash samples on stage 1, stage 7 and stage 10 for all three coals, respectively; these stages have a 50% aerodynamic cutoff diameter of 0.0324 μm, 0.973 μm and 7.33 μm, respectively. The images of stage 1 at a magnification of 250,000 showed that the particles are coagulated. The particles on stage 7 and stage 10 showed the typical spherical shape of coal ashes. There were no differences in shape for all particles, for the different combustion environments (O_2/N_2 and O_2/CO_2) or for the different O_2 concentrations. This spherical surface looked smooth and had approximately the appropriate collection diameters for each stage. However, smaller size particles were found adhered to some large particles surfaces on stage 7 and 10.

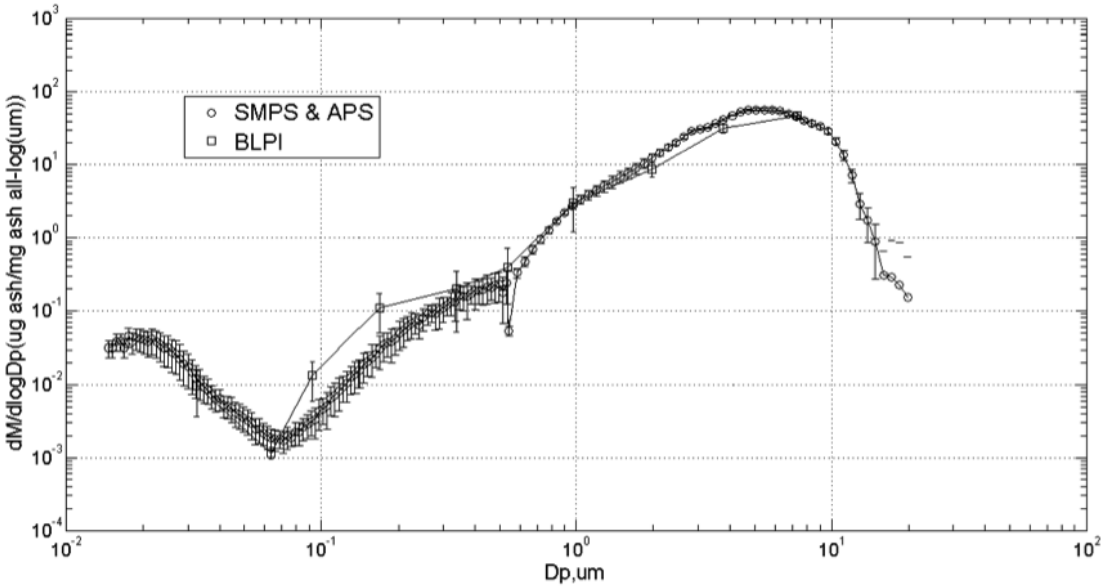

Figure 4.1: The BLPI and SMPS/APS PSDs of Utah Skyline under 21% O_2/CO_2 at 1500 K.

Table 4.1: Total collected mass distribution

				Ultrafine mode		Fine mode		Coarse mode	
	Furnace Temperature (K)	O_2 volume (%)		Mean D_p (μm)	Mass concentration (mg/g_ash)	Mean D_p (μm)	Mass concentration (mg/g_ash)	Mean D_p (μm)	Mass concentration (mg/g_ash)
Utah Skyline	1373	21	O_2/N_2	0.023	1.11	0.318	13.95	3.996	984.94
			O_2/CO_2	0.020	0.16	0.313	3.51	4.237	996.33
		31.5	O_2/N_2	0.035	9.18	0.322	7.52	4.033	983.30
			O_2/CO_2	0.028	2.13	0.296	4.34	4.317	993.21
	1500	21	O_2/N_2	0.028	1.29	0.352	5.53	4.542	993.18
			O_2/CO_2	0.023	0.83	0.343	4.28	4.657	994.89
		31.5	O_2/N_2	0.046	12.59	0.383	12.95	4.821	974.46
			O_2/CO_2	0.029	7.63	0.321	21.49	4.696	970.87
PRB	1373	21	O_2/N_2	0.056	6.27	0.39	1.58	3.874	992.15
			O_2/CO_2	0.032	1.52	0.329	1.39	4.271	997.09
		31.5	O_2/N_2	0.075	14.19	0.435	2.39	3.312	983.42
			O_2/CO_2	0.055	4.43	0.382	1.15	3.763	994.42
	1500	21	O_2/N_2	0.053	6.03	0.351	1.84	3.936	991.95
			O_2/CO_2	0.034	2.99	0.336	2.63	4.411	994.38
		31.5	O_2/N_2	0.067	10.75	0.379	2.69	3.651	986.56
			O_2/CO_2	0.045	3.41	0.342	2.08	4.136	994.51
Illinois #6	1373	21	O_2/N_2	0.028	16.44	0.333	11.27	3.972	972.30
			O_2/CO_2	0.025	8.82	0.353	7.60	4.36	983.58
		31.5	O_2/N_2	0.041	56.47	0.354	16.97	4.065	926.56
			O_2/CO_2	0.030	17.03	0.349	13.33	5.305	969.64
	1500	21	O_2/N_2	0.027	6.72	0.863	97.71	5.672	895.58
			O_2/CO_2	0.024	4.45	0.913	100.64	6.138	894.92
		31.5	O_2/N_2	0.037	14.19	0.787	92.32	6.068	893.49
			O_2/CO_2	0.036	15.05	0.841	72.34	6.229	912.61

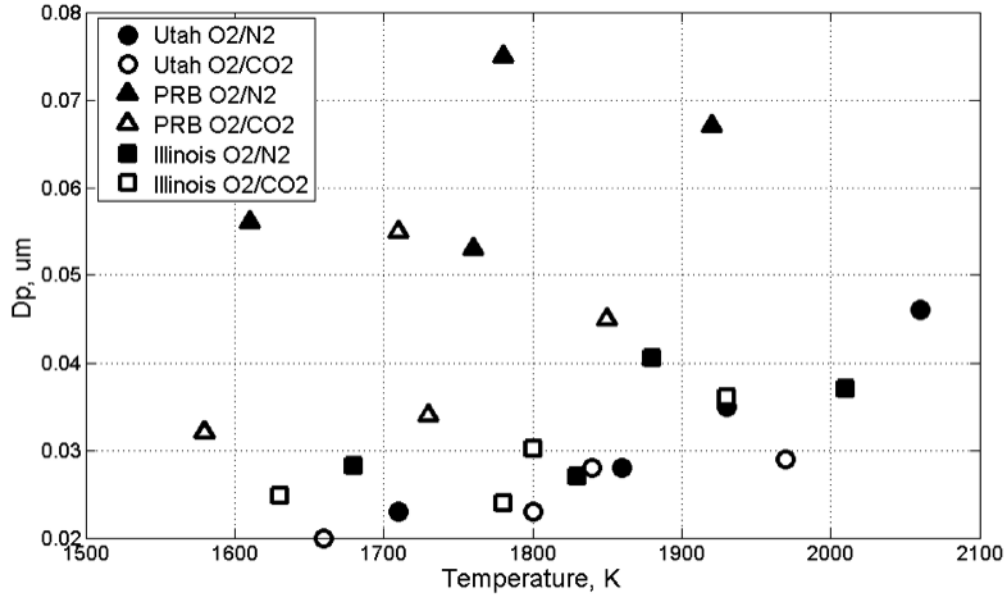

Figure 4.2: The mean size of ultrafine particles.

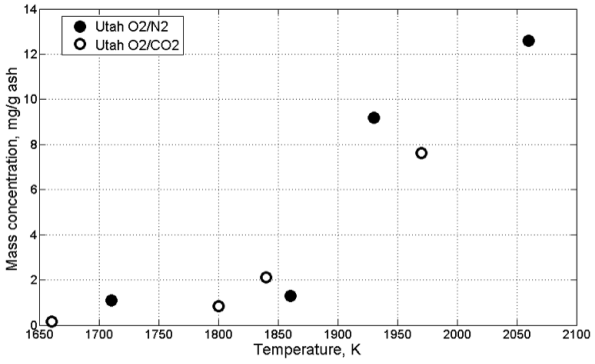

(a) Mass concentration of ultrafine particle for Utah Skyline for all conditions.

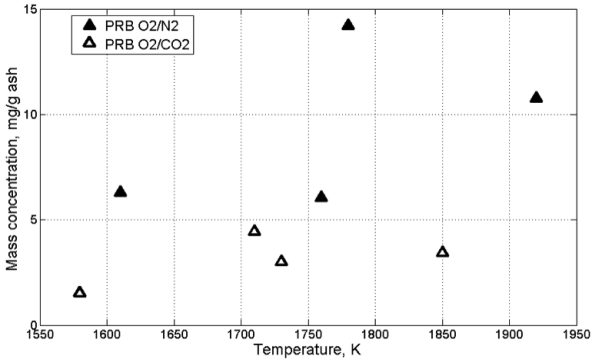

(b) Mass concentration of ultrafine particle for PRB for all conditions.

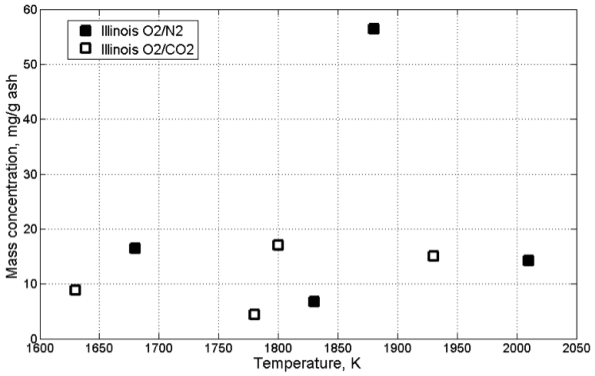

(c) Mass concentration of ultrafine particle for Illinois #6 for all conditions.

Figure 4.3: The total mass of ultrafine particles for Utah Skyline (a), PRB (b), and Illinois #6 (c).

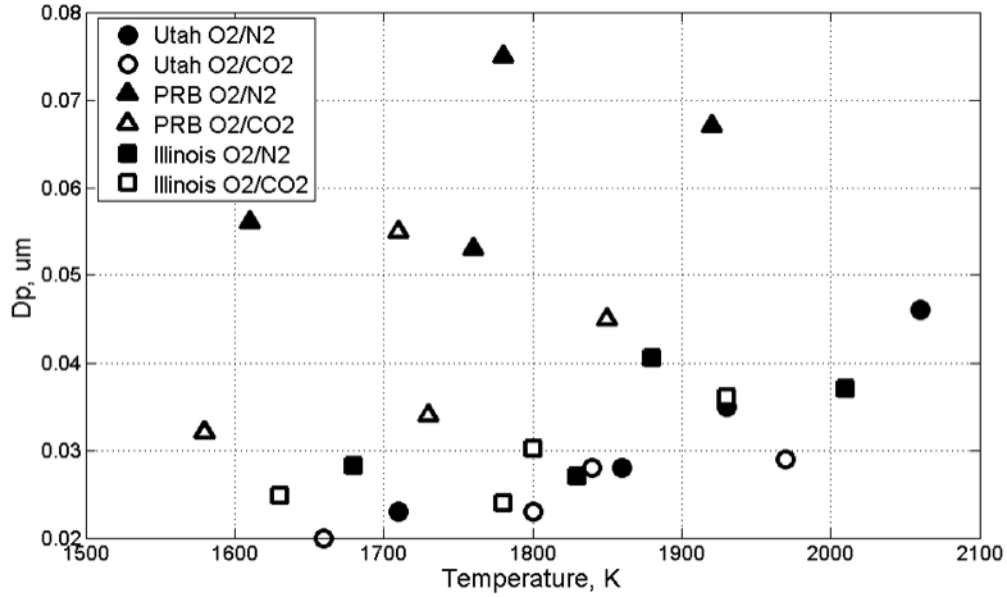

Figure 4.4: The mean size of fine particles for all coals.

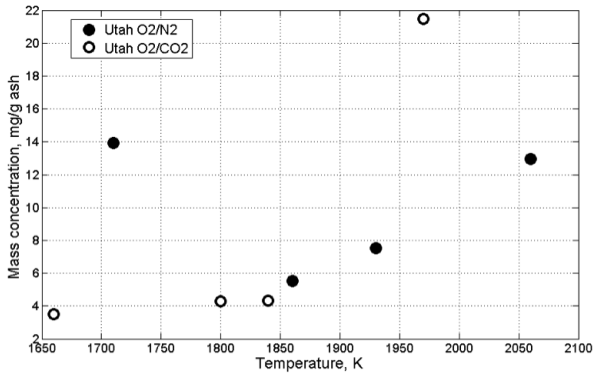

(a) Mass concentration of fine particle for Utah Skyline for all conditions.

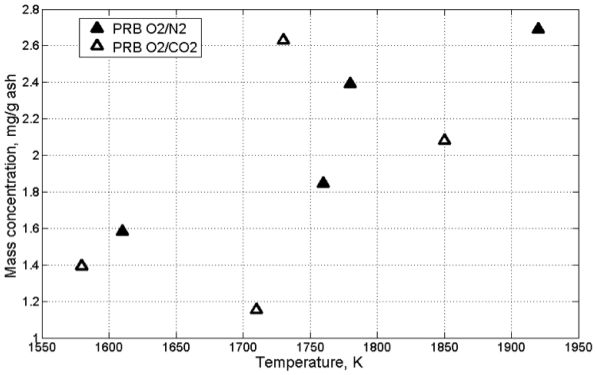

(b) Mass concentration of fine particle for PRB for all conditions.

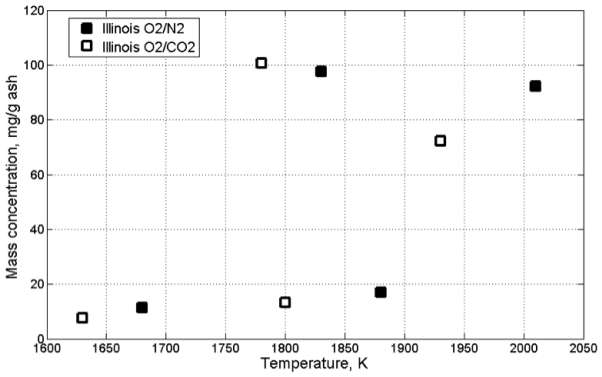

(c) Mass concentration of fine particle for Illinois #6 for all conditions.

Figure 4.5: The total mass of fine particles for Utah Skyline (a), PRB (b), and Illinois #6 (c).

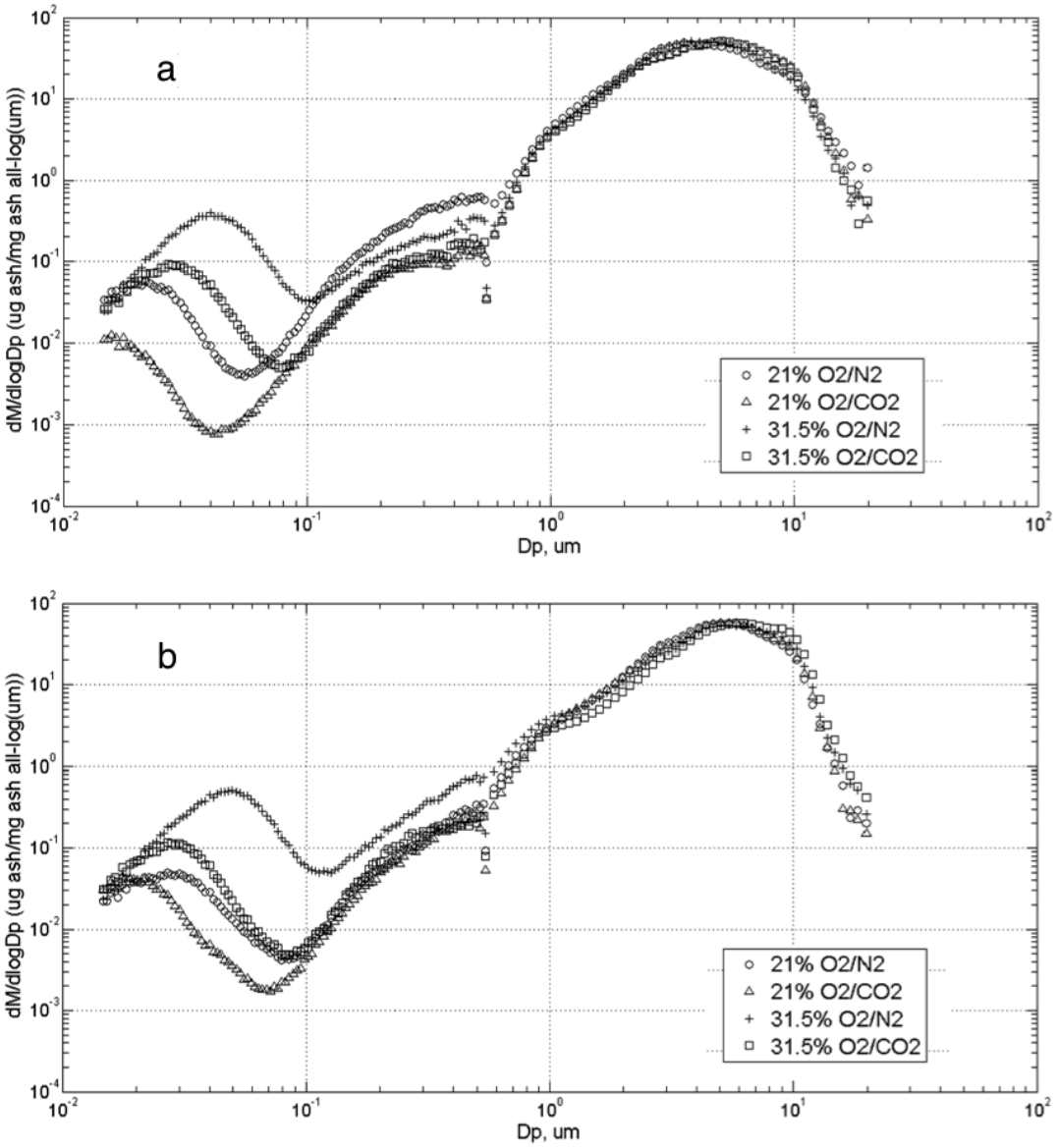

Figure 4.6: PSDs of Utah Skyline at 1373 K (a) and 1500 K (b).

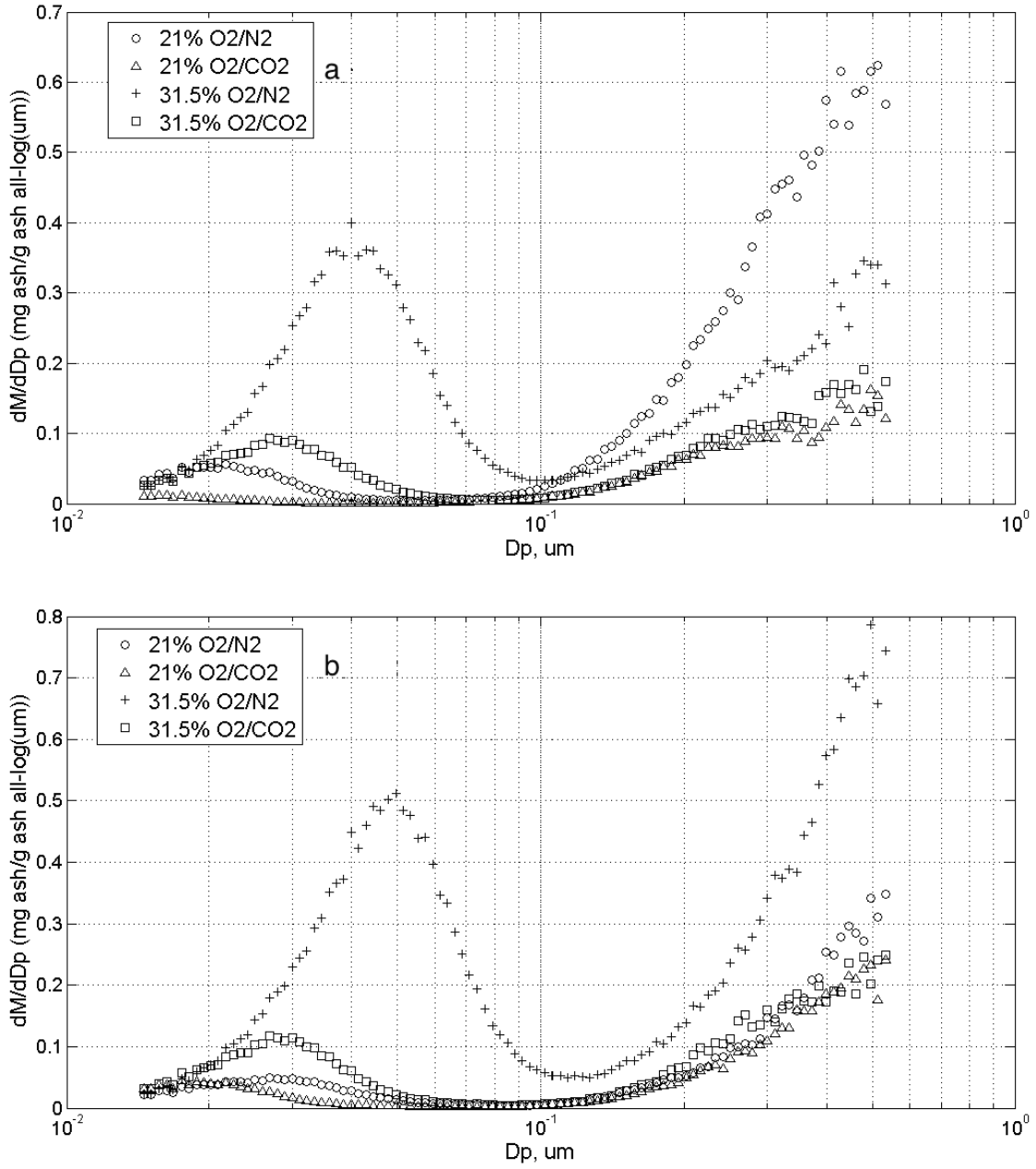

Figure 4.7: Normal plot of PSDs of ultrafine and fine particles of Utah Skyline coal at 1373 K (a) and 1500 K (b).

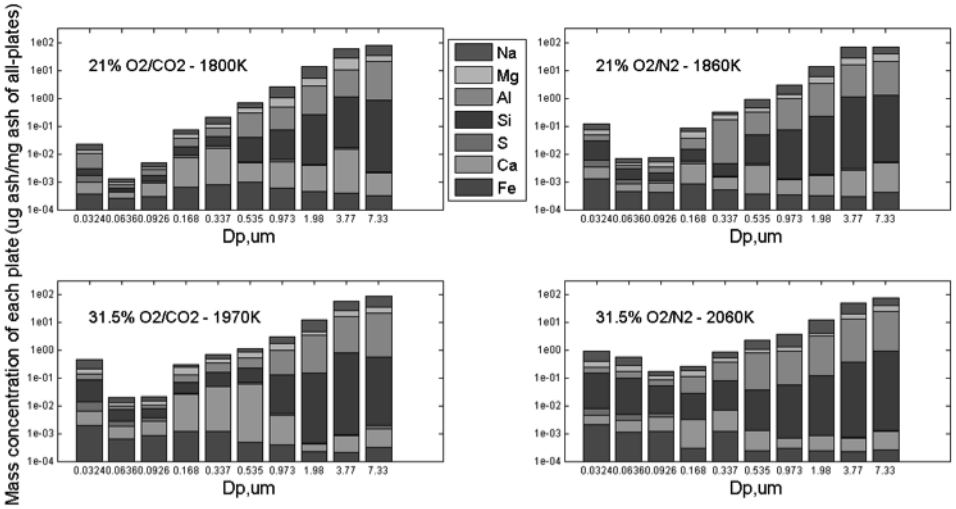

Figure 4.8: Elemental mass fraction size distribution of Utah Skyline at 1500 K. Temperatures are predicted maximums from the simulation.

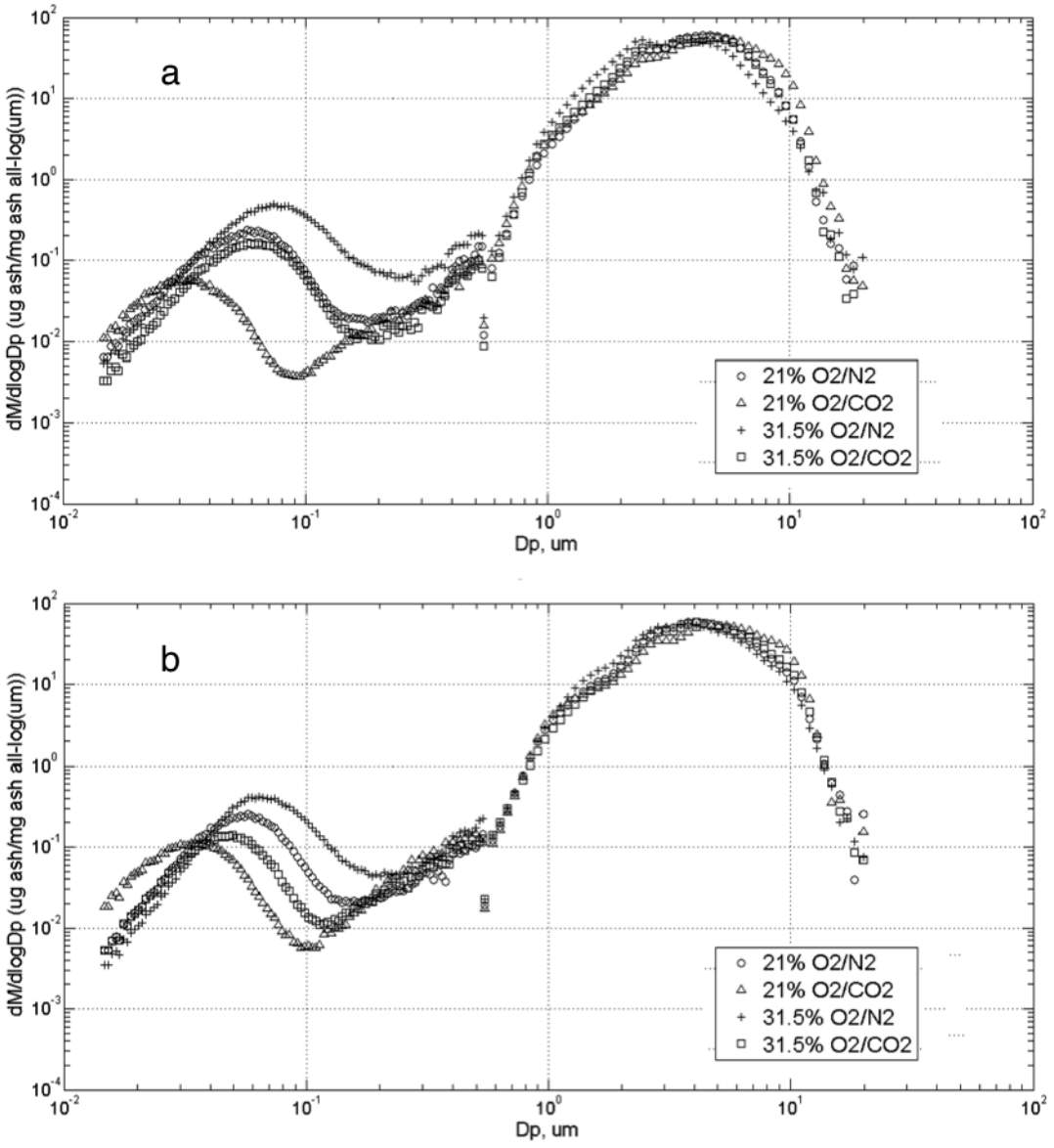

Figure 4.9: PSDs of PRB at 1373 K (a) and 1500 K (b).

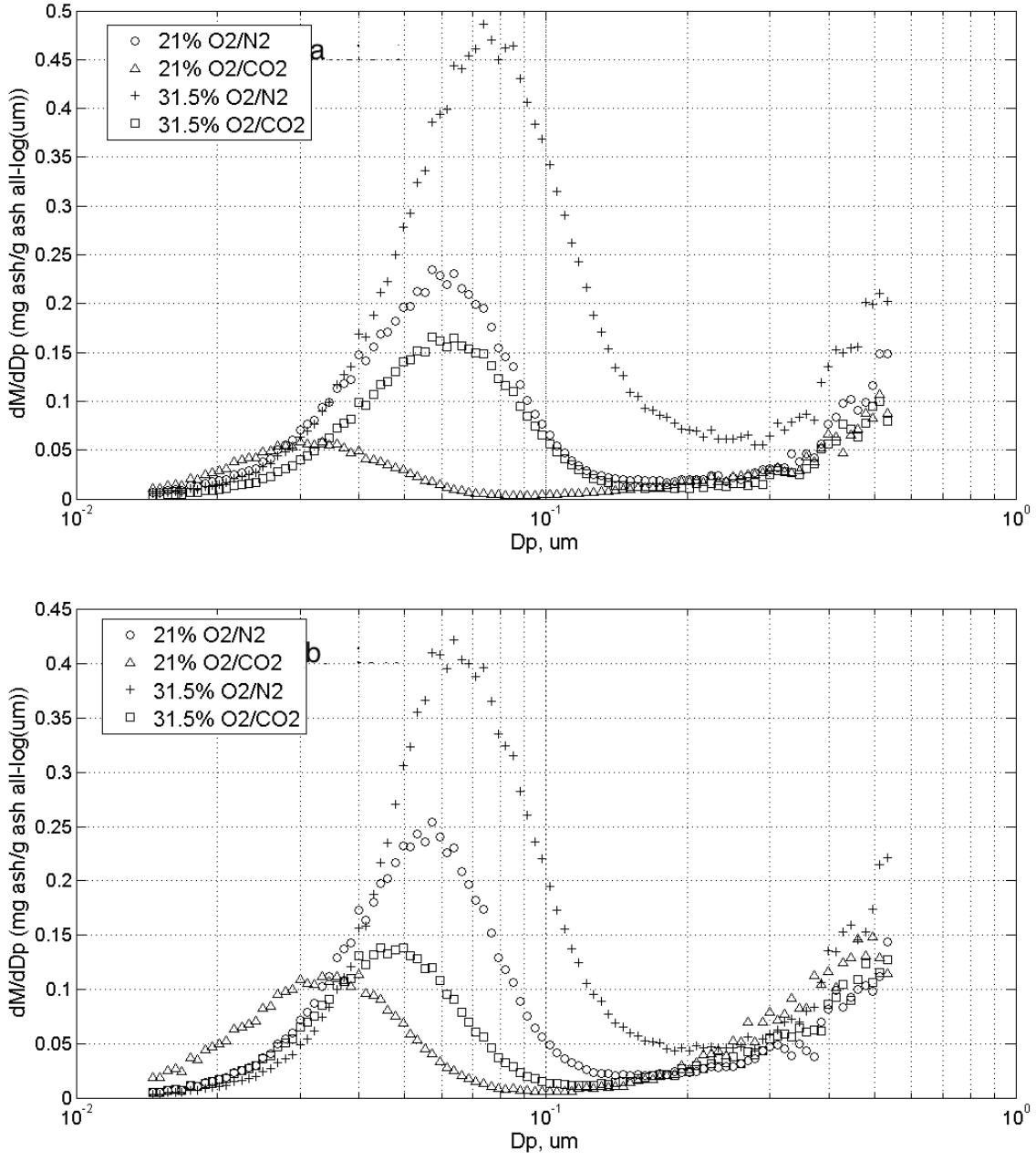

Figure 4.10: Normal plot of PSDs of ultrafine and fine particles of PRB coal at 1373 K (a) and 1500 K (b).

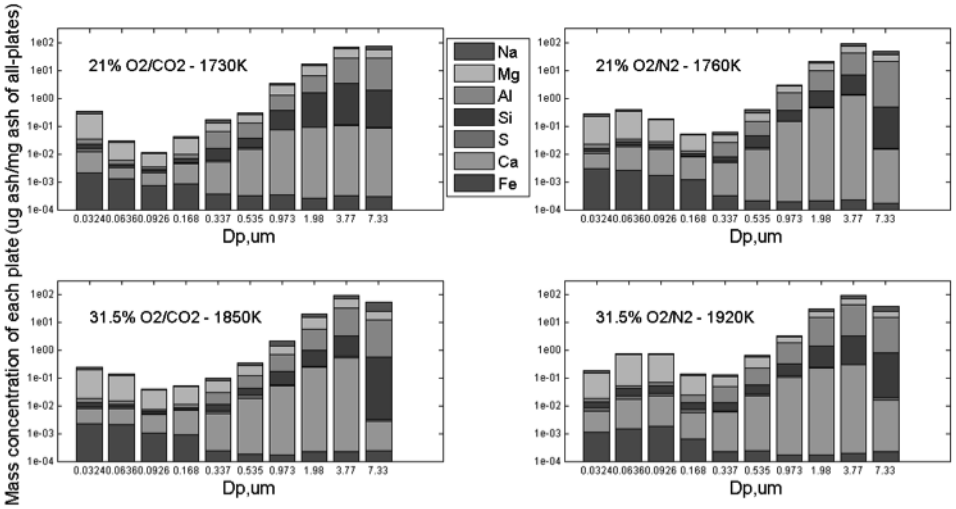

Figure 4.11: Elemental mass fraction size distribution of PRB at 1500 K. Temperatures are predicted maximums from the simulation.

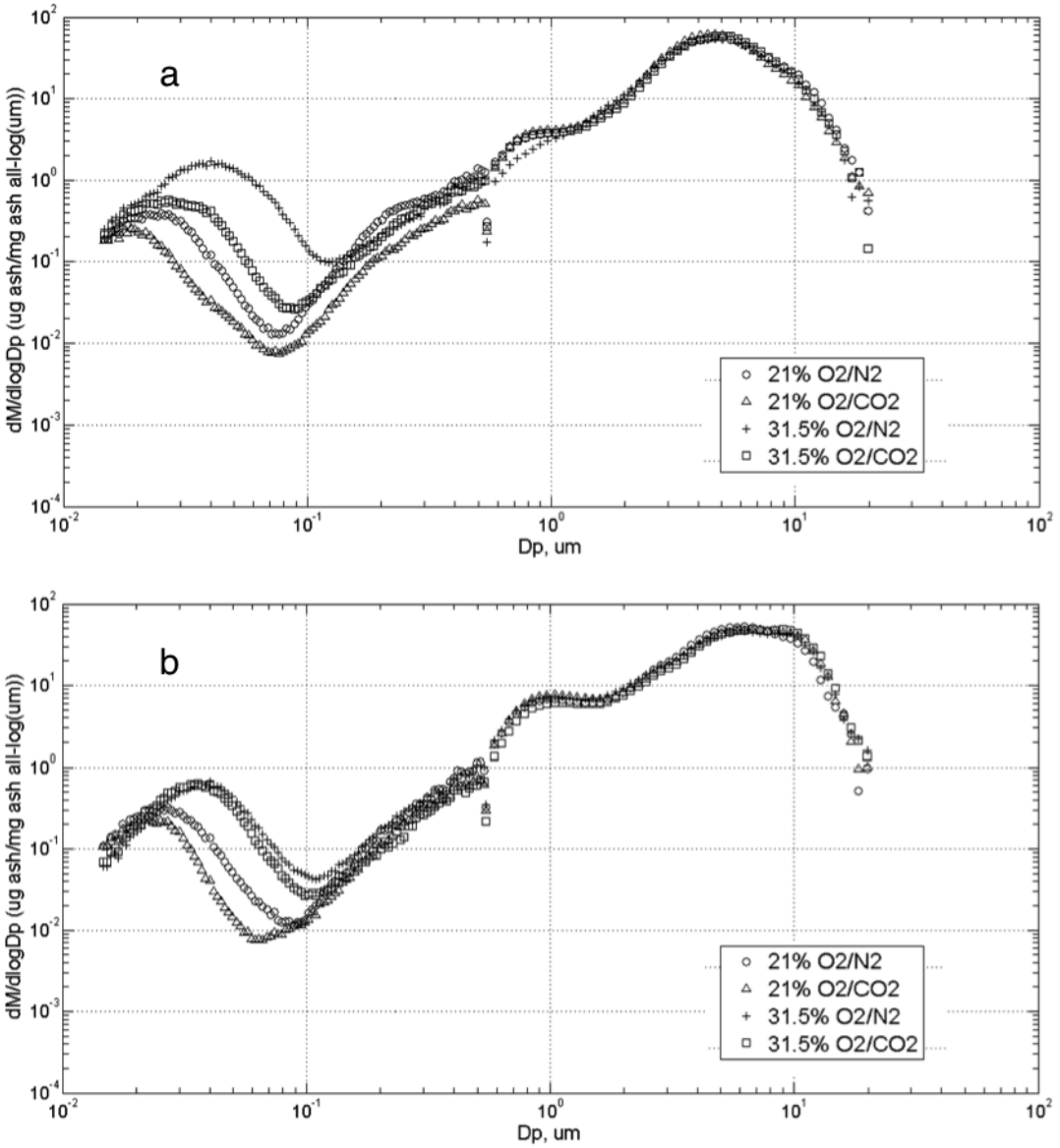

Figure 4.12: PSDs of Illinois #6 at 1373 K (a) and 1500 K (b).

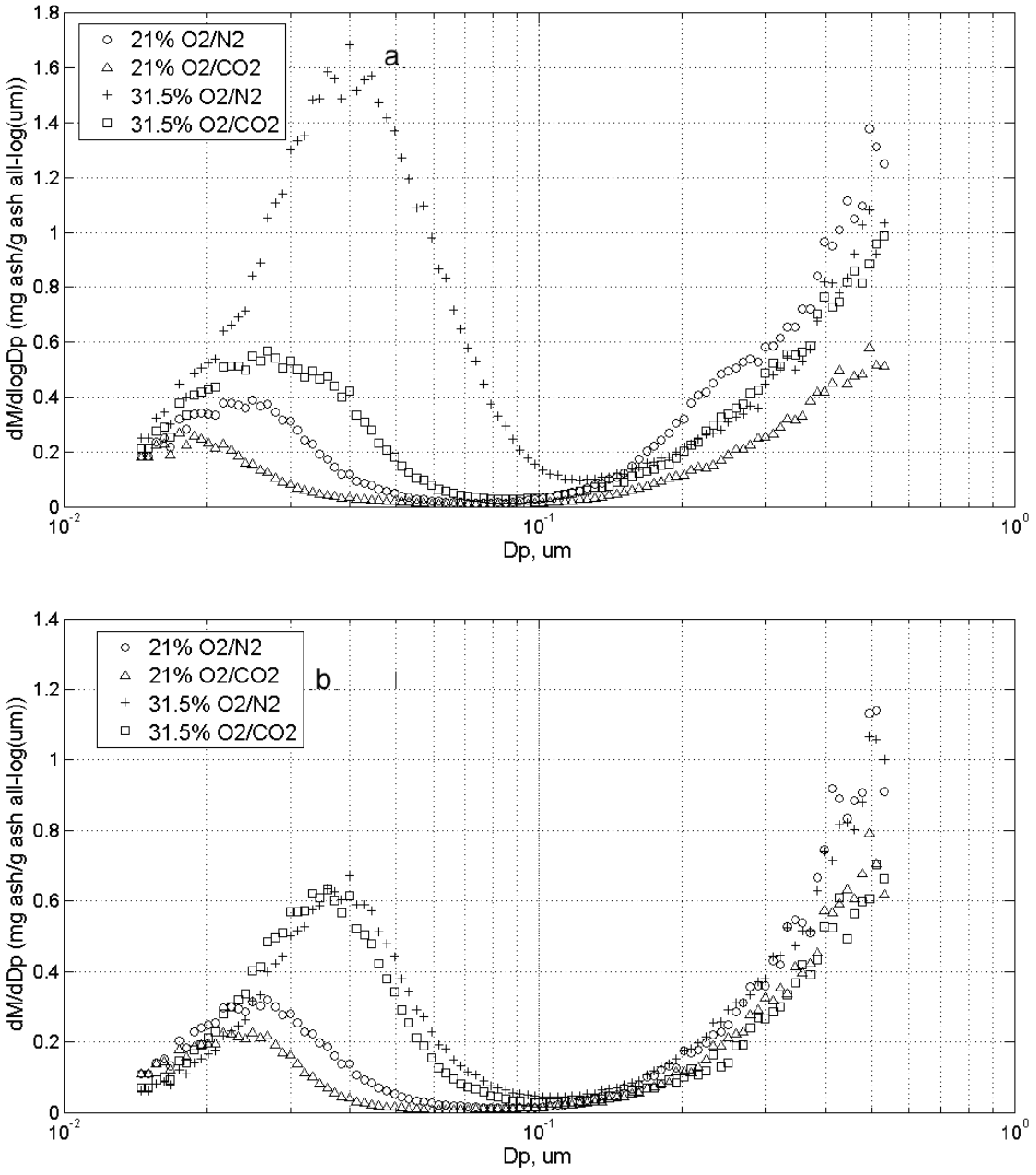

Figure 4.13: Normal plot of PSDs of ultrafine and fine particles of Illinois #6 coal at 1373 K (a) and 1500 K (b).

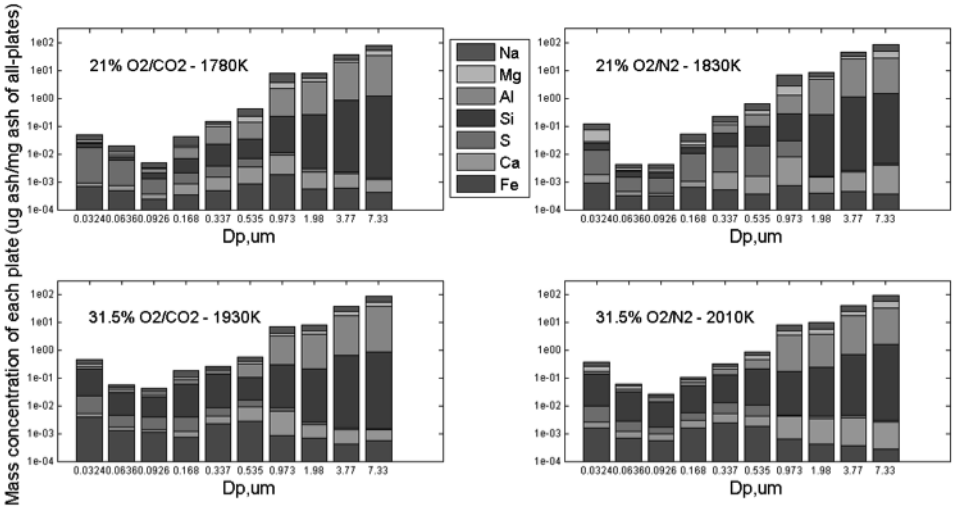

Figure 4.14: Elemental mass fraction size distribution of Illinois #6 at 1500 K. Temperatures are predicted maximums from the simulations.

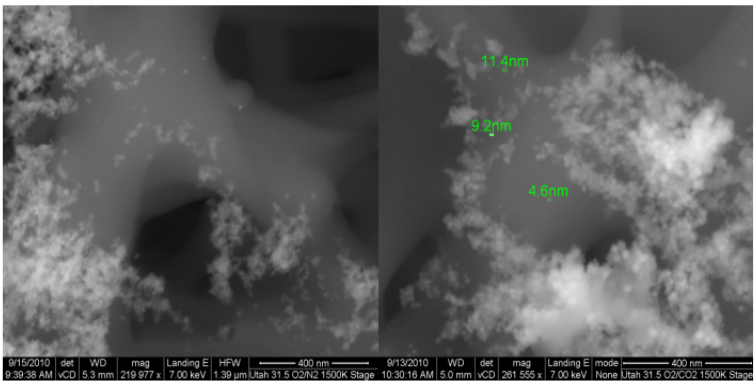

(a)

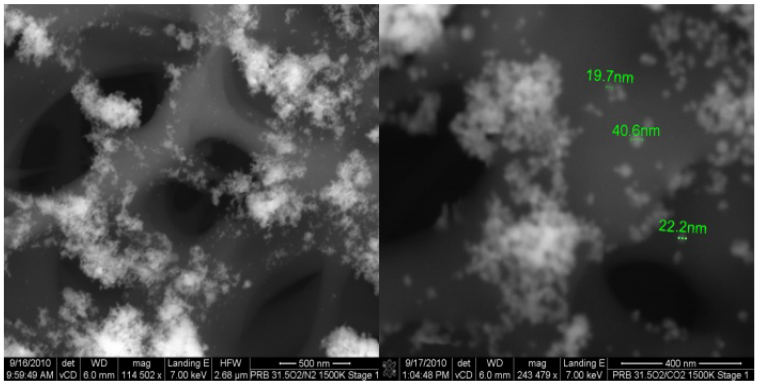

(b)

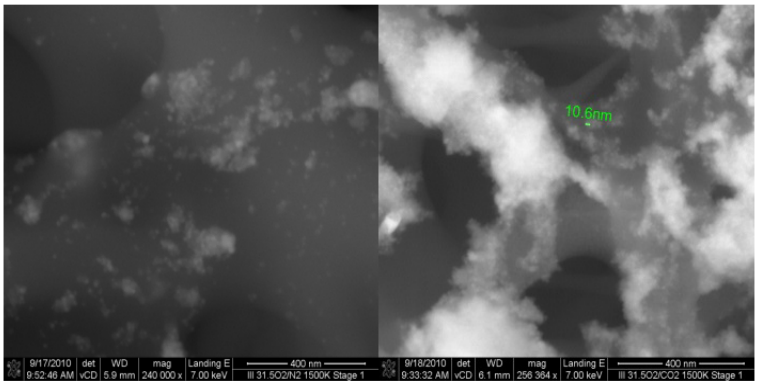

(c)

Figure 4.15: Morphology at Stage 1 of Utah Skyline (a), PRB (b) and Illinois #6 (c) combusted under 31.5% O_2/CO_2 and 31.5% O_2/N_2 conditions at 1500 K. (part 1/3)

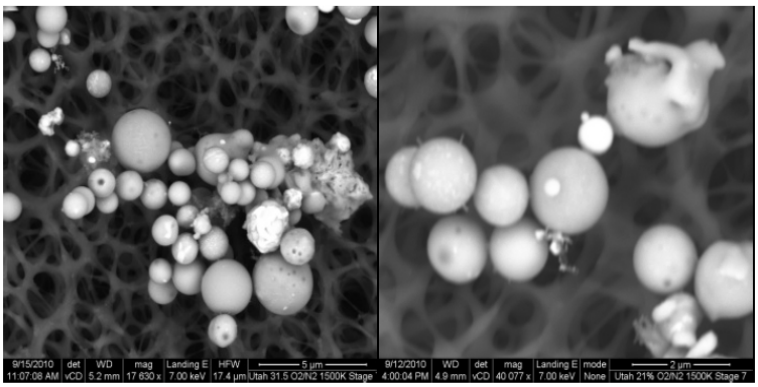

(a)

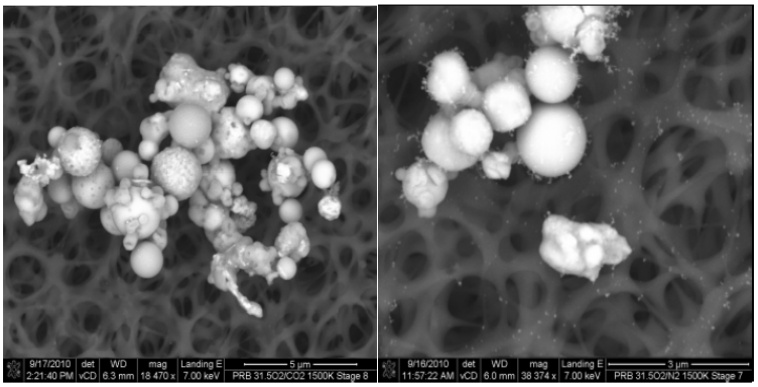

(b)

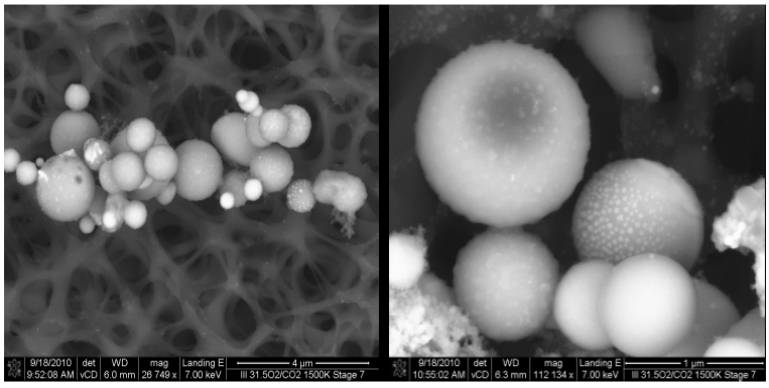

(c)

Figure 4.16: Morphology at Stage 7 of Utah Skyline (a), PRB (b) and Illinois #6 (c) combusted under 31.5% O_2/CO_2 and 31.5% O_2/N_2 conditions at 1500 K. (part 2/3)

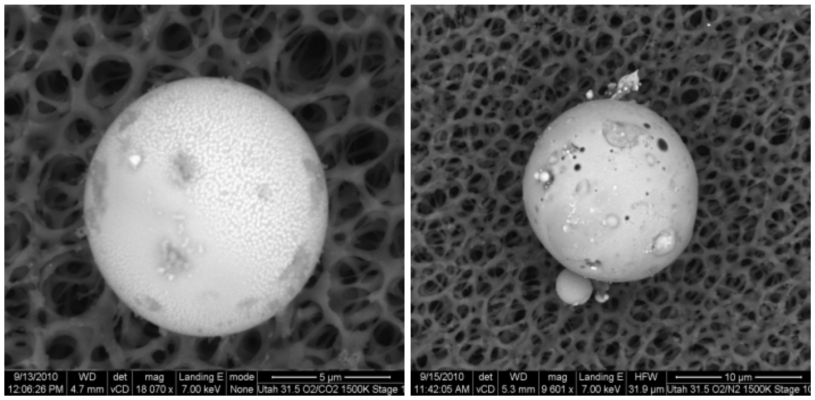

(a)

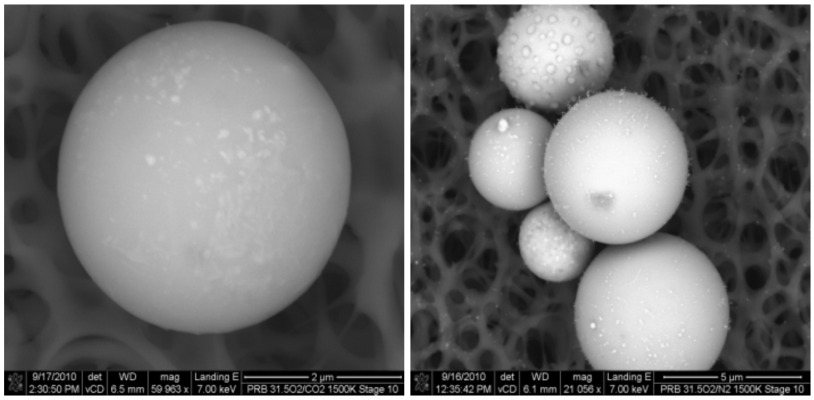

(b)

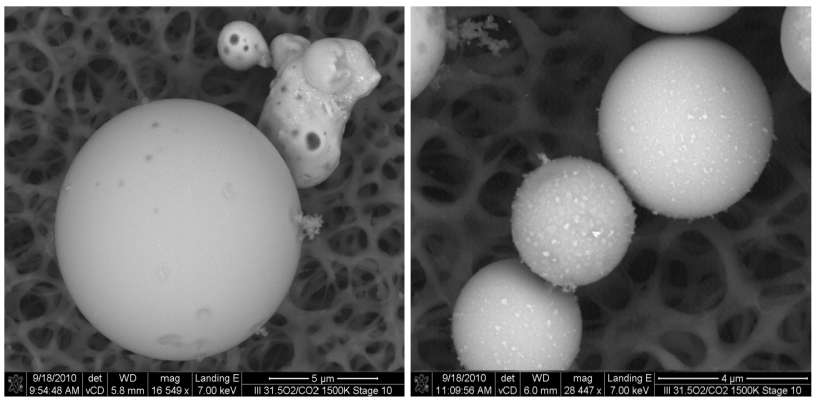

(c)

Figure 4.17: Morphology at Stage 10 of Utah Skyline (a), PRB (b) and Illinois #6 (c) combusted under 31.5% O_2/CO_2 and 31.5% O_2/N_2 conditions at 1500 K. (part 3/3)

CHAPTER 5

CONCLUSIONS

This thesis focused on an experimental study of particulate formation of pulverized coal under the well-controlled experimental conditions of a laboratory laminar flow furnace. The effects of furnace temperature, gas composition and coal type on ash particulate formation in an O_2/N_2 and O_2/CO_2 environment were studied. SMPS/APS data showed that particle temperature was the dominant factor for the amount of ultrafine particle formation. Increasing the particle temperature by increasing the O_2 concentration significantly yielded an increase in mass. The yields of particulates from O_2/CO_2 combustion were less than those from O_2/N_2 combustion for all three coals. The studies suggested that CO_2 significantly reduced ash particle formation formed by decreasing refractory oxide vaporization and by decreasing temperature. The simulation results indicated that increasing the furnace temperature and O_2 concentration enhanced the ash particle generation due to increased predicted particle combustion temperature. Combustion in an O_2/CO_2 environment also yielded smaller mean particle sizes in the ultrafine and fine modes as compared to an O_2/N_2 combustion environment with same O_2 concentration.

EDS results supported the SMPS/APS data and showed that, the coarse composition did not change significantly for the coals, but the ultrafine compositions were dependent upon the silicon, for Utah, and calcium, for PRB contents.

APPENDIX

SIMULATION MODEL CODE

A.1 Temperature and Burnout Model for Single Coal Char Combustion

In the experimental studies of ash formation, particular focus lied in the analysis of the combustion temperature. The preliminary project of this model is to predict char temperature change with the combustion conditions that capture char combustion characteristics but exhibit the lowest possible complexity.

This model program is able to calculate coal char particle temperature profiles, solid mass concentration and burnout time for coal char combusted in a gaseous environment at pseudo-steady state. This program was designed for one-dimensional, spherical particle, no boundary layer geometry studies. This program included calculations for various coal char particle sizes, combustion gas compositions, furnace temperature and coal types. Both chemical kinetics and mass diffusion of gases on the surface of char particle were included in this program. The theoretical bases for this single coal char combustion temperature and burnout model was discussed in Chapter 3.

A.2 Single Coal Char Particle Model Code

A Matlab code was developed to execute the temperature, particle concentration and burnout time calculation. The accuracy of the calculation result is highly dependent on thermal, reaction kinetics data. The first part of the program was the calculation of all thermal and chemical reaction parameters. Then, the program coupled heat transfer, chemical reaction and mass transport on the surface of the particle to get temperature profile and mass consumption profile.

The following code was used for computing 65 micron Utah Skyline char particle combusted at 21% O_2/CO_2 at a furnace temperature of 1373 K. Results for other

combustion conditions can be calculated with inputting correct parameters.

```
function dy = ratefuncT1373O21OC(t,y)
Tp = y(1);
mp = y(2);

dp = 32.5E-6;          % Particle radius (m)
Cp = 992.88;           % Specific heat of coal J/kg.K:
                       % Utah Skyline 992.88;
                         PRB 1188.6;
                         Illinois #6 1042.44
rho = 1531.8;          % kg/m^3   Utah Skyline 1531.8;
                                  PRB 1533.1;
                                  Ill 1532.0

Vp = 4/3*pi*dp^3;

Epsilon = 0.8;          % Particle emissivity
Sigma = 5.67E-08; % The Stefan-Boltzmann constant W/m^2.K^4
Ap = 4*pi*dp^2;        % The particle surface area (m^2)
Tw = 1373;             % Wall temperature K
Tg = Tw;               % Gas temperature = wall temperature

 % Calculation for heat transfer coefficient
xO2 = 0.21;              % O2 concentration
kO2 = 0.07300;         % Thermal conductivity of gases
kN2 = 0.0607;
kCO2 = 0.0581;

k0 = xO2*kO2+(1-xO2)*kCO2;  % Initial thermal conductivity
                              of gas mixture
Nu = 2;                      % Nusselt number
T0 = 900;                   % Initial temperature of particle
k = k0*((Tp+Tg)/(2*T0))^0.75; %    The relation of thermal
                              conductivity and temperature
h = Nu*k/(2*dp); % Calculation for heat transfer coefficient

deltahst = 9.25E+6;   % 9250 kJ/kg-C
deltaHst = deltahst*0.4939;  % Fix carbon:
                               Utah Skyline 0.4939,
                               PRB 0.3801,
                               Illinois #6 0.4558

% Calculation for Diffusion coefficient
c = 0.00266;             % Chapman-Enskog equation constant
```

```
Pconv = 1.01325;     % Furnace pressure
P = 1;
Pbar = P*Pconv;       % Calculate with bar

sigO2 = 3.467;          % Characteristic length, A
sigN2 = 3.798;
sigCO2 = 3.941;
epO2 = 106.7;            % K
epN2 = 71.4;
epCO2 = 195.2;

sigbi = (sigO2+sigCO2)/2;
epbi = (epO2*epCO2)^0.5;

Tm = (Tp+Tg)/2;
Tstar = Tm/epbi;

A = 1.06036;
B = 0.15610;
C = 0.19300;
D = 0.47635;
E = 1.03587;
F = 1.52996;
G = 1.76474;
H = 3.89411;

omegaD = A/((Tstar)^B)+C/exp(D*Tstar)
         +E/exp(F*Tstar)+G/exp(H*Tstar);

MO2 = 32;                % Molar mass, g/mol
MN2 = 28;
MCO2 = 44;
Mbi = 2/(1/MO2+1/MCO2);

Dbi = c*(Tm^1.5)/Pbar*(Mbi^0.5)*(sigbi^2)*omegaD);
                          % Diffusion coefficient of O2

Rg = 82.06;     % The universal gas constant atm.cm3/mol.K
phi = 2;                    % Mechanism factor CO2=1; CO=2
kd = 24*phi*Dbi/(2*dp*10*Rg*Tm);
                         % Diffusion rate coefficient of O2

%Calculation for reaction rate, Arrhenius equation
A = 600;                    % m/s
E = 17150;                % J/mol
```

```
R = 1.986;                  % J/mol.K
e = exp(1);
kp = A*e^(-E/(R*Tp));  % Reaction rate coefficient

P = 1;
PO2 = P*xO2;

dy = zeros(2,1);      % A column vector
dy(1) = (-Epsilon*Sigma*Ap*(Tp^4-Tw^4)-Ap*h*(Tp-Tg)
        +deltaHst*PO2/(1/kd+1/kp)*Ap)/(mp*Cp);
                                % Energy balance equation
dy(2) = -PO2/(1/kd+1/kp)*Ap;       % Mass balance equation

mp_0=rho*4/3*pi*dp^3;   % Initial particle mass
Tp_0=900;                  % Initial particle temperature
[T,Y] = ode15s(@ratefuncT1373O21OC,[Tp_0 mp_0]);
                                 % Solving for the equations
```

REFERENCES

[1] Act, A. Clean Air Act Amendments, Federal Register, Section. *Federal Register, Section* (1990), 301–366.

[2] Altrichter, D. M. *Optical determination of time-temperature profiles for single particle coal conbustion*. PhD thesis, Massachusetts Institute of Technology, Department of Chemical Engineering, 1981.

[3] Bachmann, J., Damberg, R., Caldwell, J., Edwards, C., and Koman, P. Review of the national ambient air quality standards for particulate matter: Policy assessment of scientific and technical information. oaqps staff paper. Final report. Tech. rep., Environmental Protection Agency, Research Triangle Park, NC (United States). Office of Air Quality Planning and Standards, 1996.

[4] Badzioch, S., Field, M., and Gregory, D. Investigation of temperature variation of thermal conductivity+ thermal diffusivity of coal. *Fuel 43*, 4 (1964), 267.

[5] Baughman, G. L. *Synthetic fuels data handbook*. Cameron Engineers, Inc., 1978.

[6] Baum, M., and Street, P. Predicting the combustion behaviour of coal particles. *Combustion Science and Technology 3*, 5 (1971), 231–243.

[7] Baxter, L. L. Char fragmentation and fly ash formation during pulverized-coal combustion. *Combustion and Flame 90*, 2 (1992), 174–184.

[8] Berner, A., and Luerzer, C. Mass size distributions of traffic aerosols at Vienna. *The Journal of Physical Chemistry 84*, 16 (1980), 2079–2083.

[9] Berner, A., Lürzer, C., Pohl, F., Preining, O., and Wagner, P. The size distribution of the urban aerosol in Vienna. *Science of the Total Environment 13*, 3 (1979), 245–261.

[10] Bird, R. B., Stewart, W. E., and Lightfoot, E. N. *Transport phenomena*. John Wiley & Sons, 2007.

[11] Block, C., and Dams, R. Study of fly ash emission during combustion of coal. *Environmental Science & Technology 10*, 10 (1976), 1011–1017.

[12] Buhre, B., Elliott, L., Sheng, C., Gupta, R., and Wall, T. Oxy-fuel combustion technology for coal-fired power generation. *Progress in Energy and Combustion Science 31*, 4 (2005), 283–307.

[13] Buhre, B., Hinkley, J., Gupta, R., Wall, T., and Nelson, P. Submicron ash formation from coal combustion. *Fuel 84*, 10 (2005), 1206–1214.

[14] Carslaw, H. S., Jaeger, J. C., et al. *Conduction of heat in solids*, vol. 2. Clarendon Press Oxford, 1959.

[15] Dockery, D. W., Pope, C. A., Xu, X., Spengler, J. D., Ware, J. H., Fay, M. E., Ferris Jr, B. G., and Speizer, F. E. An association between air pollution and mortality in six us cities. *New England Journal of Medicine 329*, 24 (1993), 1753–1759.

[16] EPA, U. Recovery Act of 1976. *Public Law 94*, 580 (1981), 90.

[17] Esmen, N. A., and Corn, M. Residence time of particles in urban air. *Atmospheric Environment (1967) 5*, 8 (1971), 571–578.

[18] Field, M. A. Rate of combustion of size-graded fractions of char from a low-rank coal between 1200 K and 2000 K. *Combustion and Flame 13*, 3 (1969), 237–252.

[19] Gavalas, G. R. Analysis of char combustion including the effect of pore enlargement. *Combustion Science and Technology 24*, 5-6 (1980), 197–210.

[20] Goetz, G., NSAKALA, Y. I., Patel, R., and Quentin, G. Combustion and gasification kinetics of chars from four commercially significant coals of varying rank. In *International Conference on Coal Science* (1983), pp. 571–574.

[21] Gordon, S., and McBride, B. J. Computer program for calculation of complex chemical equilibrium compositions, rocket performance, incident and reflected shocks, and chapman-jouguet detonations. *NASA Reference Publication* (1976).

[22] Haynes, B. S., Neville, M., Quann, R. J., and Sarofim, A. F. Factors governing the surface enrichment of fly ash in volatile trace species. *Journal of Colloid and Interface Science 87*, 1 (1982), 266–278.

[23] Helble, J., and Sarofim, A. Influence of char fragmentation on ash particle size distributions. *Combustion and Flame 76*, 2 (1989), 183–196.

[24] Hillamo, R. E., and Kauppinen, E. I. On the performance of the berner low pressure impactor. *Aerosol Science and Technology 14*, 1 (1991), 33–47.

[25] Howard, J., and Essenhigh, R. Pyrolysis of coal particles in pulverized fuel flames. *Industrial & Engineering Chemistry Process Design and Development 6*, 1 (1967), 74–84.

[26] Incropera, F. P. *Fundamentals of heat and mass transfer*. John Wiley & Sons, 2011.

[27] Kang, S.-G., Helble, J. J., Sarofim, A. F., and Beér, J. M. Time-resolved evolution of fly ash during pulverized coal combustion. In *Symposium (International) on Combustion* (1989), vol. 22, Elsevier, pp. 231–238.

[28] Kauppinen, E. I., and Pakkanen, T. A. Coal combustion aerosols: A field study. *Environmental Science & Technology 24*, 12 (1990), 1811–1818.

[29] Lemmon, E., McLinden, M., and Huber, M. Nist standard reference database 23, nist thermodynamic properties of refrigerants and refrigerant mixtures database (refprop), version 7.0. *National Institute of Standards and Technology* (2002).

[30] Lighty, J. S., Veranth, J. M., and Sarofim, A. F. Combustion aerosols: Factors governing their size and composition and implications to human health. *Journal of the Air & Waste Management Association 50*, 9 (2000), 1565–1618.

[31] Linak, W. P., Miller, C. A., Seames, W. S., Wendt, J. O., Ishinomori, T., Endo, Y., and Miyamae, S. On trimodal particle size distributions in fly ash from pulverized-coal combustion. *Proceedings of the Combustion Institute 29*, 1 (2002), 441–447.

[32] Linak, W. P., Miller, C. A., and Wendt, J. O. Comparison of particle size distributions and elemental partitioning from the combustion of pulverized coal and residual fuel oil. *Journal of the Air & Waste Management Association 50*, 8 (2000), 1532–1544.

[33] Marrero, T., and Mason, E. A. Gaseous diffusion coefficients. *Journal of Physical and Chemical Reference Data 1*, 1 (1972), 3–118.

[34] Mulcahy, M., and Smith, I. The kinetics of combustion of pulverized coke, anthracite, and coal chars. *Rev. Pure and Applied Chemistry 19* (1969), 81–108.

[35] Neville, M., Quann, R., Haynes, B., and Sarofim, A. Vaporization and condensation of mineral matter during pulverized coal combustion. In *Symposium (International) on Combustion* (1981), vol. 18, Elsevier, pp. 1267–1274.

[36] Nsakala, N., Marion, J., Bozzuto, C., Liljedahl, G., Palkes, M., Vogel, D., Gupta, J., Guha, M., Johnson, H., and Plasynski, S. Engineering feasibility of co2 capture on an existing us coal-fired power plant. In *First National Conference on Carbon Sequestration* (2001), pp. 15–17.

[37] Poling, B. E., Prausnitz, J. M., and O'connell, J. P. *The Properties of gases and liquids*, vol. 5. McGraw-Hill New York, 2001.

[38] Quann, R., and Sarofim, A. Vaporization of refractory oxides during pulverized coal combustion. In *Symposium (International) on Combustion* (1982), vol. 19, Elsevier, pp. 1429–1440.

[39] Quann, R. J. *Ash vaporization under simulated pulverized coal combustion conditions*. PhD thesis, Massachusetts Institute of Technology, 1982.

[40] Ramsden, A. A microscopic investigation into the formation of fly-ash during the combustion of a pulverized bituminous coal. *Fuel 48*, 2 (1969), 121–137.

[41] Sarofim, A. F., Howard, J. B., and Padia, A. S. The physical transformation of the mineral matter in pulverized coal under simulated combustion conditions. *Combustion Science and Technology 16*, 3-6 (1977), 187–204.

[42] Seames, W. S., and Wendt, J. O. Partitioning of arsenic, selenium, and cadmium during the combustion of Pittsburgh and Illinois #6 coals in a self-sustained combustor. *Fuel Processing Technology 63*, 2-3 (2000), 179 – 196.

[43] Senior, C., and Flagan, R. Ash vaporization and condensation during combustion of a suspended coal particle. *Aerosol Science and Technology 1*, 4 (1982), 371–383.

[44] Sheng, C., Li, Y., Liu, X., Yao, H., and Xu, M. Ash particle formation during O2/CO2 combustion of pulverized coals. *Fuel Processing Technology 88*, 11 (2007), 1021–1028.

[45] Simons, G. A., and Finson, M. L. The structure of coal char: Part I-pore branching. *Combustion Science and Technology 19*, 5-6 (1979), 217–225.

[46] Smith, I. The combustion rates of coal chars: A review. In *Symposium (International) on Combustion* (1982), vol. 19, Elsevier, pp. 1045–1065.

[47] Smith, I. W. The intrinsic reactivity of carbons to oxygen. *Fuel 57*, 7 (1978), 409–414.

[48] Smith, R. D., Campbell, J. A., and Nielson, K. K. Concentration dependence upon particle size of volatilized elements in fly ash. *Environmental Science & Technology 13*, 5 (1979), 553–558.

[49] Speight, J. G. *Handbook of coal analysis*, vol. 166. John Wiley & Sons, 2005.

[50] Szekely, J., Evans, J. W., and Sohn, H. Y. *Gas-solid reactions*. Academic Press, 1976.

[51] Tognotti, L., Longwell, J., and Sarofim, A. The products of the high temperature oxidation of a single char particle in an electrodynamic balance. In *Symposium (International) on Combustion* (1991), vol. 23, Elsevier, pp. 1207–1213.

[52] Weast, R. C. Handbook of chemistry and physics. *The American Journal of the Medical Sciences 257*, 6 (1969), 423.

[53] Xie, R., Seip, H. M., Wibetoe, G., Nori, S., and McLeod, C. W. Heavy coal combustion as the dominant source of particulate pollution in Taiyuan, China, corroborated by high concentrations of arsenic and selenium in PM 10. *Science of the Total Environment 370*, 2 (2006), 409–415.